CENTRO DE INVESTIGACIÓN Y DE ESTUDIOS AVANZADOS
DEL INSTITUTO POLITÉCNICO NACIONAL

UNIDAD ZACATENCO
DEPARTAMENTO DE FÍSICA

“Restringiendo no unitariedad en procesos cargados de violación de sabor y en neutrinos de colisionador”

Tesis que presenta

Jesús Miguel Celestino Ramírez

para obtener el Grado de

Doctor en Ciencias

en la Especialidad de

Física

Director de tesis: Dr. Omar Gustavo Miranda Romagnoli

Ciudad de México Enero, 2025

CENTER FOR RESEARCH AND ADVANCED STUDIES OF THE NATIONAL POLYTECHNIC INSTITUTE

UNIT ZACATENCO
PHYSICS DEPARTMENT

"Constraining non unitary in charged lepton flavor violation processes and collider neutrinos"

by

Jesús Miguel Celestino Ramírez

In order to obtain the

Doctor of Science

degree, speciality in

Physics

Advisor: Ph. D. Omar Gustavo Miranda Romagnoli

Mexico City January, 2025

Agradecimientos

Con profunda estima me gustaría agradecer al Dr. Omar Miranda por su paciencia e invaluable guía através de estos 5 años de doctorado, así como por su papel en mi formación como investigador. También deseo agradecer al Dr Gabriel López Castro, Dr. Abdel Pérez Lorenzana, Dr. Josué De Santiago Sanabria y al Dr. Eduardo Peinado Rodríguez por sus valiosos comentarios y sus preguntas que enriquecieron este trabajo.

Agradezco a mi familia por todo el apoyo emocional y las palabras de aliento que me impulsaron a terminar el doctorado.A mi madre, Zaida, por brindarme su amor, cariño incondicional y su optimismo ante las adversidades. A mi padre, Miguel Ángel, por nuestras enriquecedoras discusiones y por compartir su perspectiva de la vida. A mis hermanos, especialmente a quique, por siempre estar al pendiente de mí. A mis abuelos, quienes me inculcaron el valor del trabajo y la confianza en mí mismo y en mis capacidades. A mi pareja, Naomi por su constante motivación amor y apoyo, y al teo y rogelio por su compañía durante el proceso de redacción de esta tesis.

Agradezco también a mis amigos del doctorado: Juan Manuel, Alejandra, Diego Portillo, César Ramos, Johan Caicedo y Jorge Gabriel por su invaluable compañía, las discusiones de física y la motivación que me brindaron.

Finalmente, agradecer al Consejo Nacional de Humanidades, Ciencias y Tecnologías (CONAHCYT) por la beca que hizo posible la realización de este doctorado. Además del proyecto CONAHCYT A1-S-23238.

Resumen

A pesar del gran éxito del Modelo Estándar, existen motivaciones para suponer que puede existir física más allá de dicho modelo. Un caso de gran relevancia es la posibilidad de que haya más estados de masa de neutrinos, tales como los leptones pesados neutros (Neutral Heavy Leptons). En este caso existirán efectos de no-unitariedad en la matriz de mezcla leptónica. Estos efectos de no-unitariedad cambian la probabilidad de oscilación de los neutrinos activos y podrían dar evidencia de nueva física. En este tesis exploramos implicaciones fenomenológicas de la no-unitariedad en experimentos actuales y futuros, tales como el detector de FASERν y los de búsqueda de decaimientos cargados con violación del sabor leptónico (cLFV). Mostraremos la relevancia de estos experimentos en la busqueda de estas señales de nueva física y sus perspectivas en el futuro.

Abstract

Despite the great success of the Standard Model, there are some motivations to think about new physics beyond the Standard Model. One case of great relevance is the possibility of new neutrino massive states, such as the Neutral Heavy Leptons (NHL). With more neutrino massive states, there are non-unitary effects in the leptonic mixing matrix. The non-unitary effects change the oscillation probability of active neutrinos, which could give evidence of new physics. This thesis explores the phenomenological implications of the non-unitary effects in current and future experiments, such as the FASERν detector and the experimental searches of charged lepton flavor violation (cLFV) processes. We will show the relevance of these experiments in searching for new physics and their future perspectives.

Contents

Chapter 1

Introduction

The Standard Model (SM) is one of the most successful theories, with its capability to explain much experimental evidence with high accuracy. The SM is a gauge theory that is conformed by three quantum field theories (QFT) and with $SU(3)_c \times SU(2)_L \times U(1)_Y$ symmetry that governs its dynamics [1]. Each QFT describes one force in the SM. The first one was the quantum electrodynamics (QED) created by Feynman, Tomonaga, Schwinger, and many others. Then, Sheldon Glashow [2], Steven Weinberg [3], and Abdus Salam [4] unified the QED with the weak interaction in the Electro-Weak theory (EW). Finally, quantum chromodynamics theory (QCD) describes strong interactions.

One of the greatest predictions of SM is the existence of the Higgs particle, which, in the EW theory, gives mass to the charged fermions and the Z and $W^{\pm}$ through the Higgs mechanism. The CMS and ATLAS detectors discovered the Higgs boson at the Large Hadron Collider (LHC) in 2012 [5, 6] and confirmed the EW predictions, giving more reliability to the theory.

Despite all the achievements the model gives us, there is some phenomenology beyond its predicted capabilities, such as the asymmetry of matter and antimatter in the universe and the nature and mass mechanism of neutrinos that have tiny masses, as evidenced by neutrino oscillations. In this work, we will explore some neutrino phenomenology to answer these questions.

Pauli postulated the neutrino as a solution to the missing energy in the beta decay. Neutrinos are one of the most copious particles in the universe; however, neutrinos weakly interact with matter, and the fact that neutrinos are chargeless particles makes their measurement more difficult. But even before the neutrino oscillation evidence, there was some description of the neutrino oscillation.

Pontecorvo was the first person to postulate the neutrino oscillation; in his vision, the neutrino oscillates between the neutrino and antineutrino as an analogy to $K^0 \leftrightarrows \bar{K}^0$ [7], since at that time, we only had measurements of one neutrino flavor. Nowadays, the neutrino oscillation theory is known to describe an oscillation between different flavors. Different experiments supported this hypothesis, but it wasn't until the Super-Kamiokande collaboration and the Sudbury Neutrino Observatory (SNO) had enough neutrino events that the oscillation theory was established. In 2015, Takaaki Kajita [8] and Arthur B. McDonald [9] were awarded the Nobel Prize in Physics "for their contributions to the discovery of neutrino oscillations, which demonstrated that neutrinos have mass".

The confirmation of neutrino oscillation opens the door to many questions, such as the nature, the mass hierarchy, and the mechanism that gives mass to the neutrinos. One way to answer these questions is to add more particles or symmetries, as in the seesaw mechanism. In the minimal seesaw, we add heavy right-handed neutrinos that would act as a messenger to give mass to the active neutrinos. In this model, all the neutrinos are Majorana particles; therefore, this mechanism not only answers about how the neutrino acquires mass but also what the nature of neutrinos is.

Adding more neutrinos to the theory will be reflected in the dimension of the neutrino mixing matrix, and these new neutrinos also have effects in the active sector of the neutrino mixing matrix. Therefore, the oscillation probability of the active neutrino is changed, and the observation of anomalies in the neutrino number of events could confirm these new particles. Of particular interest is the effect due to non-unitary; as mentioned above, we would detect this effect in the neutrino events independently of the model, making such signatures in neutrino experiments a very appealing subject. The relation of specific seesaw models with the model-independent non-unitary parameters would be equally interesting. In this work, we will test the non-unitary effects in different schemes. We will use several observables that would be useful to constrain the non-unitary parameters. Examples of this are the analysis of the neutrino events in the future FASERν detector that we will discuss in this work or the study of a theoretical model as the low-scale seesaw combined with the charged lepton flavor violation limits to restrict the non-unitary parameter space. In the literature, we can see other works in a similar direction [10–18].

The manuscript's structure is as follows: In chapter 2, we will talk about the SM particle content and the interaction that we will be interested in. Then, we will com-

pute the oscillation probability and describe the model-independent parametrization of the neutrino mixing matrix in chapter 3. In chapter 4, we study the seesaw type I mechanism and how it works using the model-independent parametrization. At the end of the chapter, we will find a match between the two parametrizations. Using the FASERν and FASERν2 data, we perform a χ^2 analysis to study the sensitivity to the non-unitary parameters in the model-independent parameterization in the chapter 5. In chapter 6, we use the linear seesaw to compute the branching ratio of $\ell_i \to \ell_j \gamma$ and use the current and future limits to restrict the non-unitary parameters and find the expected future sensitivity. We also use the matching between different parametrizations to translate these limits to the model-independent parametrization. Afterward, we use the limits of the processes and the limits of the non-unitary parameters that came from oscillation experiments to do a combined analysis for the seesaw type I in chapter 7. Finally, in chapter 8, we present a summary and the conclusions of the work.

Chapter 2

The Standard Model Particle Content, its Interactions, and Lagrangian

The Standard Model (SM) is a gauge theory with a symmetry group of $SU(3)_c \otimes SU(2)_L \otimes U(1)_Y$, where the index c is for color, L is for left-handed chirality, and Y is the hypercharge. The SM is described by two quantum field theories: Quantum Chromodynamics (QCD), which governs the strong interaction, and the Electroweak (EW) theory, which unifies the weak interaction with the Quantum Electrodynamics (QED). The group's generators correspond to the gauge boson fields, which mediate the forces between particles. For the SM, we have 12 bosons that govern the dynamics of the different Quantum field theories (QFT). QCD is in charge of processes such as hadronization. In this case, the conserved charge is the color; we have eight bosons called gluons in this gauge theory. In the case of the electroweak (EW) theory, there are four generators before spontaneous symmetry breaking, corresponding to the gauge fields (A^i_μ) (associated with the $SU(2)_L$ group) and (B_μ) (associated with the $U(1)_Y$ group). After spontaneous symmetry breaking, these gauge fields mix to form the well-known physical bosons: ($W^\pm$), (Z^0), and the photon (γ). The $W^\pm$ bosons mediate charged weak interactions, the Z^0 boson mediates neutral weak interactions, and the photon mediates electromagnetic interactions. The following section will introduce the 12 fundamental fermions that interact in the SM.

2.1 Standard Model Particle Content

The SM particle content consists of the bosons, which carry the different forces, and the fermions that are coupled to the bosons. The bosons fulfill the Bose-Einstein statistics. In other words, these particles could be in the same quantum state as

other bosons. On the other hand, the fermions follow the Fermi-Dirac statistics and cannot be in the same quantum state; this is called the Pauli exclusion principle. The fermions are grouped into two categories: quarks and leptons; for each case, the particle's spin is $\frac{1}{2}$. In the leptonic sector, we have the electrons (e), muons (μ), taus (τ), and their respective neutrinos for each family (ν_e,ν_μ,ν_τ). In the SM, neutrinos are electrically neutral particles, and the other leptons have the fundamental electric charge. We can see the physical properties of the leptons in Table 2.1. The neutrinos only interact in the weak processes and, for this reason, only couple with $W^\pm$ and Z^0 bosons. The charged leptons participate in the weak and electromagnetic processes, so they can also couple with the γ.

	Leptons			
	Particles	Q	mass [GeV]	I_{W_3}
First family	Electron (e)	-1	0.511 x 10^3	$-\frac{1}{2}$
	Electron neutrino (ν_e)	0	$<10^{-9}$	$+\frac{1}{2}$
Second family	Muon (μ)	-1	105.658x10^{-3}	$-\frac{1}{2}$
	Muon neutrino (ν_μ)	0	$<10^{-9}$	$+\frac{1}{2}$
Third family	Tau (τ)	-1	1.777	$-\frac{1}{2}$
	Tau neutrino (ν_τ)	0	$<10^{-9}$	$+\frac{1}{2}$

Table 2.1: The physical properties and quantum numbers of the Standard Model lepton sector. Here, Q is the electric charge, and I_{W_3} is the third component of weak isospin. All the information is extracted from the particle data group (PDG) [19].

On the other hand, quarks are also particles with spin $\frac{1}{2}$ and are charged particles with a fraction of the fundamental charge. In the SM, we have six quarks: up (u), down (d), charm (c), strange (s), top (t), and bottom (b). We can see its physical properties in Table 2.2 which has more details. The quarks have a color charge and, for this reason, interact with the gluons. The quarks also participate in the electroweak interaction. However, we can not see free quarks due to the color confinement. Confinement restricts us to observing only color-singlet states in nature. Combinations of quarks make these states, and the particles composed of quarks are known as hadrons. Hadrons are further classified into two categories: mesons, which consist of a quark-antiquark pair, and baryons, which consist of three quarks. Finally, the last ingredient of SM is the Higgs boson. This boson gives mass, through the Higgs mechanism, to the $W^\pm$ and Z^0 bosons and also provides mass to the charge fermion particles. A typical representation of the SM appears in Fig. 2.1

	Quarks			
	Particles	Q	mass [GeV]	I_{W_3}
First family	Up (u)	$+\frac{2}{3}$	2.2 x 10^{-3}	$+\frac{1}{2}$
	Down (d)	$-\frac{1}{3}$	4.7×10^{-3}	$-\frac{1}{2}$
Second family	Muon Charm(c)	$+\frac{2}{3}$	1.27	$+\frac{1}{2}$
	Strange (s)	$-\frac{1}{3}$	96×10^{-3}	$-\frac{1}{2}$
Third family	Top (t)	$+\frac{2}{3}$	173.21	$+\frac{1}{2}$
	Bottom (b)	$-\frac{1}{3}$	4.18	$-\frac{1}{2}$

Table 2.2: The physical properties and quantum numbers of the Standard Model quark sector, where Q is the electric charge and I_{W_3} is the third component of weak isospin. All the information is extracted from the particle data group (PDG) [19].

2.2 The Dirac Equation

The fermions in the SM have spin $\frac{1}{2}$. The equation of motion that describes this kind of particle is the Dirac Equation. We can write it as [1, 20, 21]:

$$(i\hbar\gamma^\mu\partial_u - mc)\psi = 0, \tag{2.1}$$

or in natural units

$$(i\gamma^\mu\partial_u - m)\psi = 0. \tag{2.2}$$

This equation of motion comes out from the Lagrangian density [20]

$$\mathcal{L}_{Dirac} = \bar{\psi}(i\gamma^\mu\partial_u - m)\psi \tag{2.3}$$

where

$$\bar{\psi} \equiv \gamma^0\psi^\dagger. \tag{2.4}$$

It is important to remark that the ψ is a spinor with four components; the first two describe the particle, while the other two the antiparticle (in Dirac representation), and the γ represents the four gamma matrices, which are:

$$\gamma^0 = \begin{pmatrix} 0_{2\times2} & 1_{2\times2} \\ 1_{2\times2} & 0_{2\times2} \end{pmatrix}, \tag{2.5}$$

$$\gamma^i = \begin{pmatrix} 0 & \sigma^i \\ -\sigma^i & 0 \end{pmatrix}, \tag{2.6}$$

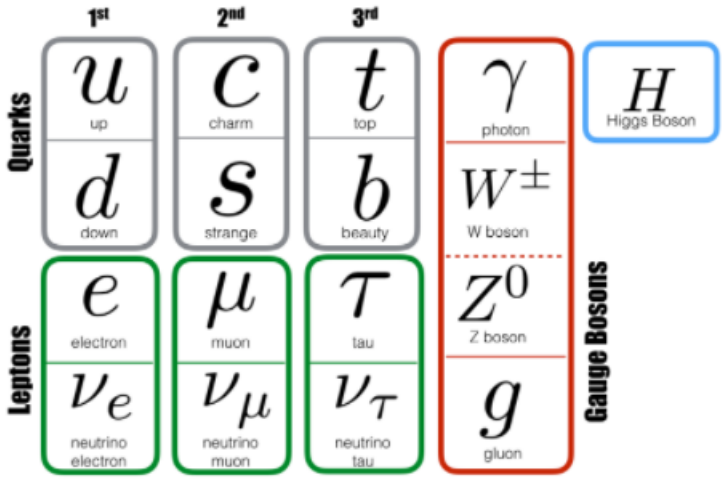

Figure 2.1: The periodic table of the SM with the fundamental particles .

where σ^i are the Pauli matrices. Also, it will be useful to define the following γ matrix:

$$\gamma^5 = i\gamma^0\gamma^1\gamma^2\gamma^3 = \begin{pmatrix} 0 & 0 & 1 & 0 \\ 0 & 0 & 0 & 1 \\ 1 & 0 & 0 & 0 \\ 0 & 1 & 0 & 0 \end{pmatrix}, \tag{2.7}$$

and in general, these matrices fulfill the following anticommutation relation:

$$\{\gamma^\mu, \gamma^\nu\} = 2\eta^{\mu\nu} I_{4\times 4}, \tag{2.8}$$

where $I_{4\times4}$ is the identity in four dimensions. This representation of the γ matrices is called the Weyl o Chiral representation. In this case, the spinor represents the two possible chiralities

$$\psi = \begin{pmatrix} \psi_L \\ \psi_R \end{pmatrix}. \tag{2.9}$$

This will be useful in the electro-weak interaction because $SU(2)$ only interacts with left-handed particles. In this context, the γ^5 is called the chirality matrix. Since it is Hermitian, the chirality is observable and it has two eigenvalues ±1. The eigenstates are the ψ_L and ψ_R

$$\gamma^5\psi_R = +\,\psi_R \tag{2.10}$$
$$\gamma^5\psi_L = -\,\psi_L \tag{2.11}$$

we can project a generic spinor field into its chiral components as:

$$\psi_R = \frac{1+\gamma^5}{2}\psi \tag{2.12}$$

$$\psi_L = \frac{1-\gamma^5}{2}\psi. \tag{2.13}$$

It is useful to define the projection operators:

$$P_R \equiv \frac{1+\gamma^5}{2}, \tag{2.14}$$

$$P_L = \frac{1-\gamma^5}{2}. \tag{2.15}$$

These operators fulfill the general condition of the projector:

$$(P_R)^2 = P_R, \tag{2.16}$$

$$(P_L)^2 = P_L, \tag{2.17}$$

and also

$$P_L + P_R = 1. \tag{2.18}$$

As a consequence, we can write every spinor as:

$$\psi = \psi_R + \psi_L. \tag{2.19}$$

Using Eqs. (2.3) and (2.19), we get the Dirac equation for each chirality

$$i\gamma^\mu \partial_\mu \psi_R = m\psi_L, \tag{2.20}$$

$$i\gamma^\mu \partial_\mu \psi_L = m\psi_R. \tag{2.21}$$

It is important to understand that this expression for the Dirac Equation only describes the dynamics of a free fermion. When we add an interaction term, it is better to consider the covariance of the Lagrangian density.

2.3 Introducing the Interactions in the Lagrangian

It is easy to notice that the Eq. (2.3) is invariant under a global phase, however, when the phase is dependent on the space-time coordinate (local symmetry) the Dirac equation is no longer invariant. To illustrate this, we describe the spinor transformation as

$$\psi'(x^\mu) = \exp(-ieQ\theta(x^\mu))\psi(x^\mu), \tag{2.22}$$

and the derivative of the spinor is:

$$\partial_\mu \psi'(x) = \exp(-ieQ\theta(x))[\partial_\mu \psi(x) - ieQ(\partial_\mu \theta)\psi(x)]. \tag{2.23}$$

Now, we compute the difference between the original Lagrangian

$$\mathscr{L}_0' - \mathscr{L}_0 = eQ(\partial_\mu \theta)\bar{\psi}(x)\gamma^\mu \psi(x). \tag{2.24}$$

If we want the Lagrangian to be invariant, we need to change the derivative to the so-called covariant derivative:

$$\mathscr{L} = \bar{\psi}(i\gamma^\mu D_u - m)\psi, \tag{2.25}$$

where

$$D_\mu = \partial_\mu + ieQA_\mu. \tag{2.26}$$

We impose that the A_μ transforms non-trivially under the transformation given in the Eq. (2.22).

$$A'_\mu = A_\mu + \partial_\mu \theta, \tag{2.27}$$

the invariance at the Lagrangian level can be seen as

$$\mathscr{L}' - eQ\bar{\psi}'(x)\gamma^\mu \psi'(x)A'_\mu = \mathscr{L} - eQ\bar{\psi}(x)\gamma^\mu \psi(x)A_\mu. \tag{2.28}$$

We recognize A_μ as the photon field. In our desire to make the Lagrangian invariant under Eq.(2.22) (U(1) symmetry), we naturally added the photon into the fermions Lagrangian. Adding the electrodynamics Lagrangian, we have:

$$\mathscr{L} = \bar{\psi}(i\gamma^\mu D_u - m)\psi - \frac{1}{4}F_{\mu\nu}F^{\mu\nu} - \frac{1}{2\xi}(\partial_\mu A^\mu)^2. \tag{2.29}$$

This is the QED Lagrangian of the SM. This Lagrangian contains the interaction between the photons and fermions. The interaction term in the Lagrangian is:

$$\mathscr{L}_{int} = -eQ\bar{\psi}\gamma^\mu \psi A_\mu. \tag{2.30}$$

This term tells us that fermion and antifermion can couple to a photon.

2.4 The Electro-Weak Interaction

In the previous section, we explained the methodology to make the Lagrangian invariant under certain symmetry. Consequently, we can naturally introduce the interaction term through the covariant derivative. However, the previous case was relatively easy because the $U(1)$ symmetry is abelian. Our purpose is to study the

neutrino interaction, and for the sake of this, we need to describe the electro-weak interaction, which symmetry is $SU(2)_L \times U(1)_Y$.

Let's describe first the $SU(2)$ symmetry, this symmetry has 3 generators that follow the angular momentum algebra:

$$[I_a, I_b] = i\epsilon_{abc} I_c. \tag{2.31}$$

The $U(1)_Y$ symmetry, also called hypercharge symmetry, is related to the charge operator and the third component of the weak isospin by the Gell-Mann-Nishijima equation:

$$Q = I_3 + \frac{Y}{2} \tag{2.32}$$

This relation already implies the unification between the weak and electromagnetic interactions. As in the last section, to have an invariant Lagrangian, we need to introduce three fields related to the $SU(2)$ and one related to the $U(1)$ in the covariant derivative

$$D_\mu = \partial_\mu + ig\vec{W}_\mu \cdot \vec{I} + ig' B_\mu \frac{Y}{2}. \tag{2.33}$$

Where W^μ and $I_i = \frac{\tau_i}{2}$ have three components. The electroweak Lagrangian takes the form [21]:

$$\begin{aligned}
\mathscr{L} =& i\bar{L_L}\gamma^\mu D_\mu L_L + i\bar{Q_L}\gamma^\mu D_\mu Q_L + \sum_{f=e,u,d} i\bar{f_R}\gamma^\mu D_\mu f_R \\
&- \frac{1}{4} W_{\mu\nu} W^{\mu\nu} - \frac{1}{4} B_{\mu\nu} B^{\mu\nu} \\
&+ (D_\mu \phi)^\dagger (D_\mu \phi) - \mu^2 \phi^\dagger \phi - \lambda(\phi^\dagger \phi)^2 \\
&- y^e(\bar{L_L}\phi e_R + \bar{e_R}\phi^\dagger L_L) \\
&- y^d(\bar{Q_L}\phi d_R + \bar{d_R}\phi^\dagger Q_L) - y^u(\bar{Q_L}\tilde{\phi} u_R + \bar{u_R}\tilde{\phi}^\dagger Q_L),
\end{aligned} \tag{2.34}$$

where ϕ is the Higgs doublet, Q is the quarks doublets, and L is the lepton doublets.

This Lagrangian is invariant under the following transformations

$$L_L \to L'_L = U^l_L(\theta(x), \eta(x)) L_L, \tag{2.35}$$
$$Q_L \to Q'_L = U^q_L(\theta(x), \eta(x)) Q_L, \tag{2.36}$$

where

$$U^l_L(\theta(x), \eta(x)) = e^{\frac{i}{2}\theta(x)\cdot\tau - \frac{i}{2}\eta(x)} \tag{2.37}$$
$$U^q_L(\theta(x), \eta(x)) = e^{\frac{i}{2}\theta(x)\cdot\tau + \frac{i}{6}\eta(x)} \tag{2.38}$$
$$U^l \text{ and } U^q \quad \epsilon \quad SU(2)_L \times U(1)_Y. \tag{2.39}$$

Also, the bosons have transformations under these symmetries. For example, B only transforms with the η function and the W^i_μ with the θ functions. As we can notice, in the Lagrangian we do not have mass terms proportional to $f\bar{f} = f_R\bar{f}_L + f_L\bar{f}_R$ because the gauge symmetry prohibits such a term. The fermions acquire mass due to the Higgs mechanism. For our purpose, we only focus on the neutrino interaction with the gauge bosons. We obtain the interaction term in the Lagrangian expanding the covariant derivate.

$$\mathscr{L}_I = -\frac{1}{2}\bar{L_L}(g\gamma^\mu \sum_i W^i_\mu \tau^i - g'\gamma^\mu B_\mu)L_L + g'\bar{e_R}\gamma^\mu B_\mu e_R, \tag{2.40}$$

where g and g' are the coupling constants of $SU(2)_L$ and $U(1)_Y$ respectivetly. We want to know what the coupling between neutrinos and bosons is. To simplify the explanation, we will focus on the electron family; however, the generalization to all families is straightforward

$$\begin{aligned}\mathscr{L}_{I,L} = &-\frac{1}{2}\begin{pmatrix}\bar{\nu_{e_L}} & \bar{e_L}\end{pmatrix}\begin{pmatrix}g\gamma^\mu W^3_\mu - g'\gamma^\mu B_\mu & g\gamma^\mu(W^1_\mu - iW^2_\mu) \\ g\gamma^\mu(W^1_\mu + iW^2_\mu) & -g\gamma^\mu W^3_\mu - g'\gamma^\mu B_\mu\end{pmatrix}\begin{pmatrix}\nu_{e_L} \\ e_L\end{pmatrix} \\ &+ g'\bar{e_R}\gamma^\mu B e_R.\end{aligned} \tag{2.41}$$

It is convenient to separate the charged (off-diagonal) and neutral (diagonal) terms. The charged part is called the Charged Current (CC) Lagrangian

$$\mathscr{L}^{CC}_{I,L} = -\frac{g}{2}(\bar{\nu}_{e_L}g\gamma^\mu(W^1_\mu - iW^2_\mu)e_L + \bar{e}_L g\gamma^\mu(W^1_\mu + iW^2_\mu)\nu_{e_L}). \tag{2.42}$$

On the other hand, the Neutral Current (NC) Lagrangian is

$$\mathscr{L}^{NC}_{I,L} = -\frac{1}{2}(\bar{\nu}_{e_L}\gamma^\mu(gW^3_\mu - g'B_\mu)e_L - \bar{e}_L g\gamma^\mu(gW^3_\mu + g'B_\mu)\nu_{e_L} - 2g'\bar{e}_R\gamma B_\gamma e_R). \tag{2.43}$$

We define a field $W^\pm_\mu$ that annihilates and creates W^+ and W^- bosons:

$$W^\pm_\mu \equiv \frac{W^1_\mu \mp iW^2_\mu}{\sqrt{2}}. \tag{2.44}$$

The Lagrangian in terms of the $W^\pm_\mu$ field is

$$\mathscr{L}^{CC}_{I,L} = -\frac{g}{\sqrt{2}}(\bar{\nu}_{e_L}\gamma^\mu W^+_\mu e_L + \bar{e}_L\gamma^\mu W^-_\mu \nu_{e_L}). \tag{2.45}$$

Using Eq. (2.15) and their properties, we can write the Lagrangian as

$$\mathscr{L}^{CC}_{I,L} = -\frac{g}{2\sqrt{2}}\bar{\nu}_e\gamma^\mu(1-\gamma^5)eW^+_\mu + H.c. \tag{2.46}$$

We can do the same for the NC Lagrangian with the next transformation

$$\begin{pmatrix} Z^\mu \\ A^\mu \end{pmatrix} = \begin{pmatrix} \cos\theta_w & -\sin\theta_w \\ \sin\theta_w & \cos\theta_w \end{pmatrix} \begin{pmatrix} W_3^\mu \\ B^\mu \end{pmatrix}, \tag{2.47}$$

where A^μ is the photon field and Z^μ is the Z^0 field and θ_W is the weak mixing angle [3]. The NC Lagrangian becomes

$$\begin{aligned} \mathscr{L}_{I,L}^{NC} = &-\frac{1}{2}(\bar{\nu}_{e_L}[(g\cos\theta_w + g'\sin\theta_w)\gamma^\mu Z_\mu + (g\sin\theta_w - g'\cos\theta_w)\gamma^\mu A_\mu]\nu_{e_L} \\ &- \bar{e}_L[(g\cos\theta_w - g'\sin\theta_w)\gamma^\mu Z_\mu + (g\sin\theta_w + g'\cos\theta_w)\gamma^\mu A_\mu]e_L \\ &- 2g'\bar{e}_R[-\sin\theta_w\gamma^\mu Z_\mu + \cos\theta_w\gamma^\mu A_\mu]e_R). \end{aligned} \tag{2.48}$$

As we know, the neutrinos do not have a coupling with the photon, so the second term in the first row of the Eq. (2.48) is zero. This leads us to the next equivalence

$$g\sin\theta_w = g'\cos\theta_w \tag{2.49}$$

$$\tan\theta_w = \frac{g'}{g}. \tag{2.50}$$

This expression relates the coupling constant with the weak mixing angle. We can rewrite the NC Lagrangian as follows

$$\begin{aligned} \mathscr{L}_{I,L}^{NC} = &\frac{g}{\cos\theta_w}[\bar{\nu}_{e_L}\gamma^\mu Z_\mu \nu_{e_L} - (1 - 2\sin^2\theta_w)\bar{e}_L\gamma^\mu Z_\mu e_L + 2\sin^2\theta_w \bar{e}_R\gamma^\mu Z_\mu e_R \\ &+ g\sin\theta_w \bar{e}\gamma^\mu A_\mu e], \end{aligned} \tag{2.51}$$

being the last term the electromagnetic one, so that coefficient should be equal to the QED coupling

$$g\sin\theta_W = e. \tag{2.52}$$

Using Eq. (2.52) and (2.49), we get

$$e = \frac{gg'}{\sqrt{g^2 + g'^2}} \tag{2.53}$$

Now we have a relation between all of the coupling constants of the theory. It is important to remark that we use only one family (e and ν_e) to exemplify the Lagrangian for NC and CC, it is straightforward to generalize the result to all the lepton families. Also, as we see in Eq.(2.34) there exists a CC and NC Lagrangian for the quarks.

2.5 Majorana Neutrinos

Massing the neutrino opens the question of what kind of particle it is. The most straightforward way to explain the neutrino mass is that the SM Higgs gives its mass (Dirac nature); however, there are other options. The seesaw mechanism in the minimal model uses right-handed neutrinos to provide mass to the active ones. In this model, all the neutrinos are Majorana particles. But what is a Majorana particle? In simple words, a Majorana particle is its antiparticle. In this sense, we remember the Eqs. (2.21) and (2.20). If the particle is massless, these equations are decoupled, and we only need one chirality to describe the whole spinor. In other words, the particle and the antiparticle have the same motion equation. This is the case of the massless neutrino in the SM. However, we want to analyze the case when the neutrino has mass. In this case, we need to consider that one of the chiral components depends on the other to have the same degrees of freedom as in the case of a massless particle. Consequently, the two chiral parts of the Dirac equation (Eqs. (2.20) and (2.21)) must describe the same thing in two ways. We are going to use the Eq. (2.21) and conjugate it

$$(i\gamma^\mu \partial_\mu \psi_L)^\dagger = (m\psi_R)^\dagger, \tag{2.54}$$

we define $\bar{\psi} = \gamma^0 \psi^\dagger$ and we will use the $\gamma^0 \gamma^{\mu^\dagger} \gamma^0 = \gamma^\mu$, $\gamma^{0^2} = I$ properties to rewrite the equation

$$-i\partial_\mu \bar{\psi}_R \gamma^\mu = m\bar{\psi}_L. \tag{2.55}$$

Now, to have the same structure as in Eq. (2.20) we need to transpose the equation above and then multiply on the left with the charge conjugation operator C. In the QFT language, the C operator transforms a particle into an antiparticle and has the property that $C\gamma^{\mu^T} C^- = -\gamma^\mu$. Now, the motion equation becomes

$$i\gamma^\mu \partial_\mu C\bar{\psi}_R^T = mC\bar{\psi}_L^T. \tag{2.56}$$

The condition for Eq. (2.56) to describe the same motion equation that Eq. (2.20) is

$$\psi_R = C\bar{\psi}_L^T. \tag{2.57}$$

The main goal of the Majorana description is to use only one chirality to describe the whole spinor, we can write the equation of motion in terms only the ψ_L

$$i\gamma^\mu \partial_\mu \psi_L = mC\bar{\psi}_L^T. \tag{2.58}$$

Now we can describe the full spinor as

$$\psi = \psi_L + \psi_R = \psi_L + mC\bar{\psi}_L^T = \psi_L + \psi_L^C. \tag{2.59}$$

As a consequence, a Majorana field can be written as

$$\psi = \psi^C. \tag{2.60}$$

In this way, it is easier to see that a Majorana particle equals the antiparticle.

2.6 Neutrino Mixing, its Components and Degrees of Freedom

As for the quarks, the flavor neutrino is composed of a massive neutrino state superposition, giving rise to the neutrino oscillation. We will discuss the oscillation probability computation in the next chapter. In this chapter, we want to introduce the matrix that matches the flavor and mass basis

$$U = \begin{pmatrix} 1 & 0 & 0 \\ 0 & c_{23} & s_{23} \\ 0 & -s_{23} & c_{23} \end{pmatrix} \begin{pmatrix} c_{13} & 0 & s_{13}e^{-i\delta_{CP}} \\ 0 & 1 & 0 \\ s_{13}e^{-i\delta_{CP}} & 0 & c_{13} \end{pmatrix} \begin{pmatrix} c_{12} & s_{12} & 0 \\ -s_{12} & c_{12} & 0 \\ 0 & 0 & 1 \end{pmatrix}, \tag{2.61}$$

where $c_{ij} \equiv \cos\theta_{ij}$, θ_{ij} are the mixing angles that are measured by all the sources (Solar, Atmospheric, Terrestrial), and the δ^{CP} is the CP violation phase. This matrix is valid when the neutrinos have a Dirac nature. If the neutrinos are Majorana particles, we need to multiply Eq. (2.61) by the matrix

$$P = \begin{pmatrix} 1 & 0 & 0 \\ 0 & e^{i\eta_1} & 0 \\ 0 & 0 & e^{i\eta_2} \end{pmatrix} \tag{2.62}$$

2.6.1 Counting of Degrees of Freedom for Dirac Neutrinos

In the case of three neutrino flavors and massive states, the neutrino mixing matrix has dimension $N = 3$ and in general $2 \times N^2$ degrees of freedom. However the neutrino mixing matrix is a unitary one, so we have N^2 constraints and therefore the degrees of freedom down to N^2. For the unitary matrix, we have mixings and phases to describe the matrix as degrees of freedom:

$$\frac{N(N-1)}{2} \qquad mixings, \tag{2.63}$$

$$\frac{N(N+1)}{2} \qquad phases. \tag{2.64}$$

However, for the Dirac neutrinos case, we can reabsorb five phases in the fields of neutrinos and the charged leptons. This reabsorption of the phases is easy to see at

the charged current level, for this reason, we write the full weak charged current

$$j = 2 \sum_{\alpha,\beta=e,\mu,\tau} \bar{\nu}_\alpha \gamma^\mu V l_\beta, \tag{2.65}$$

where

$$V = U^{\nu\dagger} \Omega^L, \tag{2.66}$$

U^ν is the neutrino mixing and Ω^L is the lepton charged mixing matrix, commonly diagonal. As we know the CC Lagrangian is invariant under a global $U(1)$, we can transform the fields as:

$$\nu_\alpha \to e^{i\psi_{\nu_\alpha}} \nu_\alpha, \quad l_\alpha \to e^{i\psi_{l_\alpha}} l_\alpha. \tag{2.67}$$

We can write the charged current as:

$$j^\mu = 2 \sum_{\alpha,\beta=e,\mu,\tau} \bar{\nu}_\alpha e^{-i\psi_{\nu_\alpha}} \gamma^\mu V e^{i\psi_{l_\alpha}} l_\beta, \tag{2.68}$$

and factorize out the muon phase from the V matrix:

$$j^\mu = 2 e^{-i(\psi_{\nu_\mu} - \psi_{l_\mu})} \sum_{\alpha,\beta=e,\mu,\tau} \bar{\nu}_\alpha e^{-i(\psi_{\nu_\alpha} - \psi_{\nu_\mu})} \gamma^\mu V e^{i(\psi_{l_\alpha} - \psi_{l_\mu})} l_\beta. \tag{2.69}$$

From this expression, we can count the number of independent phases that we can eliminate from the mixing matrix. Besides, the phase that we have factorized out, there are other four phases in this expression, two for the subindex e ((N-1) phases if $N = 3$) and the other two for the τ subindex. All these five phases can be absorbed and we will have, for $N = 3$

$$1 + (N-1) + (N-1) = 2N - 1 = 5, \tag{2.70}$$

now, we subtract this number of degrees from our total number of parameters, N^2 and we get the physical degrees of freedom for this case:

$$N^2 - (2N - 1) = 4. \tag{2.71}$$

For that reason, the neutrino mixing has only 3 mixings and one phase. This procedure can be extended for the case of more neutrino families.

2.6.2 Counting of Degrees of Freedom for Majorana Neutrinos

For the Majorana case, the counting of degrees of freedom is slightly different since the mass term does not conserve the leptonic number, in other words, the Majorana

neutrino Lagrangian is not invariant under the global $U(1)$ and we cannot reabsorb $2N-1$ phases. We can describe the Majorana mass term as:

$$\begin{aligned}\mathscr{L}^{M}_{mass} =& \frac{1}{2}\bar{\nu^{C}}_{L}\nu_{L} + H.c. \\ =& -\frac{1}{2}m(\nu_{L}^{T}C^{\dagger}\nu_{L} + v_{L}^{\dagger}Cv_{L}^{*})\end{aligned} \tag{2.72}$$

We know that the Majorana particles are the same as the antiparticle, as a consequence the mass term does not conserve the Lepton number and for that reason, we can write the Right-handed spinor in terms of the Left-handed one. Another way to observe this statement is that we can not absorb the same number of phases in this case. We can use the following transformation to exemplify:

$$\nu_{L} \to e^{i\phi}\nu_{L}, \tag{2.73}$$

Then, the Lagrangian takes the form

$$\mathscr{L}^{M}_{mass} = -\frac{1}{2}m(e^{2i\phi}\nu_{L}^{T}C^{\dagger}\nu_{L} + e^{-2i\phi}v_{L}^{\dagger}Cv_{L}^{*}), \tag{2.74}$$

as we can see, we can not factorize the phase; consequently, it is not invariant under $U(1)$. The mass term does not allow us to absorb phases in the left-handed neutrino spinors, so we can only absorb phases using the charged Lepton spinors and the total degrees of freedom in the Majorana neutrino case is $N^2-3=6$. From these 6 degrees of freedom, 3 are mixing and 3 are phases. In the next chapter, we will describe the degrees of freedom when we add more Majorana neutrinos to the formalism using the symmetric parametrization.

Chapter 3

The Neutrino Mixing Matrix Parametrizations in the Standard Model and Beyond

In the late 1950s, Pontecorvo made the first attempt to describe neutrino oscillations, postulating an oscillation between the neutrino and the antineutrino, inspired by the analogy with Kaon oscillations. This idea was a natural hypothesis at the time, as only the electron neutrino flavor had been experimentally observed. Later, in the late 1960s, with the Homestake experiment by Raymond Davis, the first evidence for a deficiency in the solar neutrino flux made the neutrino oscillation hypothesis gain more importance and relevance. Still, it was not until the Super Kamiokande and the SNO experiments that the neutrino oscillation was confirmed. In this chapter, we want to describe the neutrino mixing matrix and the neutrino oscillation formalism in different parametrizations.

3.1 The PMNS Standard Parametrization

The most common way to describe the mixing neutrino matrix is the Particle Data Group (PDG) parametrization

$$U = R_{23}(\theta_{23}; 0)R_{13}(\theta_{13}; \delta)R_{12}(\theta_{12}; 0)P, \tag{3.1}$$

where R is a rotation matrix with their corresponding mixing angle and, in the case of R_{13}, with a CP violation phase as follows

$$R_{13}(\theta_{13}; \delta) = \begin{pmatrix} \cos\theta_{13} & 0 & \sin\theta_{13}e^{-i\delta} \\ 0 & 1 & 0 \\ -\sin\theta_{13}e^{i\delta} & 0 & \cos\theta_{13} \end{pmatrix}. \tag{3.2}$$

P is a diagonal matrix with two Majorana phases and is needed if neutrinos have a Majorana nature

$$P = diag(1, e^{i\alpha}, e^{i\beta}). \tag{3.3}$$

The full mixing matrix takes the form:

$$U = \begin{pmatrix} c_{12}c_{13}e^{i\alpha} & s_{12}c_{13}e^{i\beta} & s_{13}e^{-i\delta} \\ -(s_{12}c_{23} + c_{12}s_{23}s_{13}e^{i\delta_{CP}})e^{i\alpha} & (c_{12}c_{23} - s_{12}s_{23}s_{13}e^{1\delta_{CP}})e^{i\beta} & s_{23}c_{13} \\ (s_{12}s_{23} - c_{12}c_{23}s_{13}e^{i\delta_{CP}})e^{i\alpha} & -(c_{12}s_{23} + s_{12}c_{23}s_{13}e^{i\delta_{CP}})e^{i\beta} & c_{23}s_{13} \end{pmatrix} P. \tag{3.4}$$

Many Beyond Standard Model (BSM) theories are interested in adding more neutrinos to the mixing matrix, like the seesaw mechanism, so we need to extend the dimensions of the matrix and add more massive neutrino states. We will discuss this case in the next section.

3.1.1 Oscillation Probability

The oscillation probability is a pure quantum effect of the neutrinos. In other words, only for time evolution, a neutrino state with a flavor α could become a neutrino with flavor β. We can describe a flavor state as a superposition of neutrino massive states

$$|\nu_\alpha\rangle = \sum_i U^*_{\alpha i}|\nu_i\rangle, \tag{3.5}$$

where U is the leptonic mixing matrix. From now on the Greek letter represents the flavor index and the Latin letter the massive index. We consider that the massive neutrino states are orthonormal:

$$\langle\nu_k|\nu_i\rangle = \delta_{ki}. \tag{3.6}$$

The fact that the mixing matrix is unitary suggests that the flavor states are orthonormal

$$\langle\nu_\alpha|\nu_\beta\rangle = \delta_{\alpha\beta}. \tag{3.7}$$

The massive states obey the Schrödinger equation and, for that reason, their evolution is described by

$$|\nu_i(t)\rangle = e^{-iE_k t}|\nu_i\rangle. \tag{3.8}$$

We can substitute equation (3.8) into equation (3.5):

$$|\nu_\alpha\rangle = \sum_i U^*_{\alpha i}e^{-iE_i t}|\nu_i\rangle, \tag{3.9}$$

the U matrix has a unitary property

$$\sum_\alpha U^*_{\alpha k}U_{\alpha i} = \delta_{ki}. \tag{3.10}$$

Therefore, we can describe the massive states in terms of flavor states. Using this idea, we describe the flavor states as:

$$|\nu_\alpha(t)\rangle = \sum_{\beta=e,\mu,\tau} \sum_k U^*_{\alpha k} e^{-iE_k t} U_{\beta k} |\nu_\beta\rangle, \tag{3.11}$$

then we can compute the amplitude

$$\langle \nu_\beta | \nu_\alpha(t)\rangle = \sum_i U^*_{\alpha i} e^{-iE_i t} U_{\beta i}. \tag{3.12}$$

Therefore, we can write the oscillation probability as

$$P_{\nu_\alpha \longrightarrow \nu_\beta} = |\langle \nu_\beta | \nu_\alpha(t)\rangle|^2 = \sum_{ki} U^*_{\alpha k} U_{\beta k} U_{\alpha i} U^*_{\beta i} e^{-i(E_k - E_i)t}. \tag{3.13}$$

Using the energy dispersion

$$E_k = \sqrt{|\vec{p}|^2 + m_k^2}, \tag{3.14}$$

and the ultra-relativistic approximation for neutrinos, we can approximate the dispersion relation as:

$$E_k \approx E + \frac{m_k^2}{2E}, \tag{3.15}$$

where we have taken advantage of that, in the ultra-relativistic case, the dispersion relation is $E = |\vec{p}|$ and we can equal the momentum with the energy. For that reason, we can obtain the next equation

$$E_k - E_i \approx \frac{\Delta m^2_{ki}}{2E} = \frac{m_k^2 - m_i^2}{2E}. \tag{3.16}$$

We can substitute Eq. (3.16) into the probability expression to get

$$P_{\nu_\alpha \longrightarrow \nu_\beta} = \sum_{ki} U^*_{\alpha k} U_{\beta k} U_{\alpha i} U^*_{\beta i} e^{-i\frac{\Delta m^2_{ki}}{2E} t}. \tag{3.17}$$

As mentioned above, we are working in the ultra-relativistic regime, where it is reasonable to approximate time and distance, $t \approx L$. We did this approximation because we have more control over the distance between the detector and the source than the propagation time in the experiment

$$P_{\nu_\alpha \longrightarrow \nu_\beta} = \sum_{ki} U^*_{\alpha k} U_{\beta k} U_{\alpha i} U^*_{\beta i} e^{-i\frac{\Delta m^2_{ki} L}{2E}}. \tag{3.18}$$

Another way to write the oscillation probability is:

$$P_{\nu_\alpha \longrightarrow \nu_\beta}(L,E) = \delta_{\alpha\beta} - 4\left[\sum_{k>i} \mathrm{Re}(U^*_{\alpha k}U_{\beta k}U_{\alpha i}U^*_{\beta i})\right]\sin^2\left(\frac{\Delta m^2_{ki}L}{4E}\right) + 2\left[\sum_{k>i} \mathrm{Im}(U^*_{\alpha k}U_{\beta k}U_{\alpha i}U^*_{\beta i})\right]\sin\left(\frac{\Delta m^2_{ki}L}{2E}\right). \tag{3.19}$$

Notice that we have computed this oscillation probability in the standard three flavor paradigm. In this case, the PDG parametrization is very useful for the description of the leptonic mixing matrix. However, for BSM theories, where we usually add several massive neutrino states, it is more convenient to use a different parametrization, as we will see in the next section.

3.2 The Symmetric Parametrization and the Non-Unitary Effects

As we have seen above, we can describe the neutrino oscillation using the PMNS matrix parametrization. However, it is not the only way to describe the leptonic mixing matrix. We want to use the symmetric parametrization that seems more intuitive as we will understand it later in the chapter. The main difference between the PMNS and the symmetric parametrization is that in the last case, each mixing has a Majorana phase. We can write the leptonic mixing matrix in the symmetric parametrization as follows [22]

$$K = \omega_{23}(\theta_{23};\phi_{23})\omega_{13}(\theta_{13};\phi_{13})\omega_{12}(\theta_{12};\phi_{12}), \tag{3.20}$$

the ω matrix has the next form:

$$\omega_{13} = \begin{pmatrix} \cos\theta_{13} & 0 & \sin\theta_{13}e^{-i\phi_{13}} \\ 0 & 1 & 0 \\ -\sin\theta_{13}e^{i\phi_{13}} & 0 & \cos\theta_{13} \end{pmatrix}, \tag{3.21}$$

where θ is the mixing angle and ϕ is the Majorana phase. We recover the CP violation phase as a linear combination of the three Majorana phases. Therefore, in this parametrization, it is easier to understand that the CP violation is related to the three families. Another advantage of this parametrization is that the effective Majorana mass in neutrinoless double beta decay is described only by Majorana phases. We are interested in extending this parametrization to an arbitrary number of neutral heavy leptons (NHL), the new mixing matrix takes the form

$$U_{n\times n} = \omega_{n-1,n} \times \omega_{n-2,n} \times \cdots \omega_{1,n} \times \cdots \omega_{23}\omega_{13}\omega_{12}. \tag{3.22}$$

This matrix describes the unitary matrix that changes the basis between the flavor and the mass basis. It is common to describe this matrix as:

$$U_{n\times n} = \begin{pmatrix} N_{3\times 3} & S_{3\times m} \\ V_{m\times 3} & T_{m\times m} \end{pmatrix}, \tag{3.23}$$

where N describes the mixing in the light sector, n=m+3, and m is the total number of extra NHL. This matrix is not the PMNS due to the extra neutrino massive states.

We can factorize these new effects which are called non-unitary effects as [15]

$$N = N^{NP}U = \begin{pmatrix} \alpha_{11} & 0 & 0 \\ \alpha_{21} & \alpha_{22} & 0 \\ \alpha_{31} & \alpha_{32} & \alpha_{33} \end{pmatrix} U. \tag{3.24}$$

It is also important to remember, that this is not the only way to describe the non-unitary effects. Besides, it is also important to notice that the NHLs do not oscillate with the light neutrinos due to their heavy masses, but their effects are present in the α parameters. The α parameters depend on the mixing and the Majorana phases as follows:

$$\begin{aligned}
\alpha_{11} =& c_{1n}c_{1n-1}c_{1n-2}\cdots c_{14} \\
\alpha_{22} =& c_{2n}c_{2n-1}c_{2n-2}\cdots c_{24} \\
\alpha_{33} =& c_{3n}c_{3n-1}c_{3n-2}\cdots c_{34} \\
\alpha_{21} =& c_{2n}c_{2n-1}\cdots c_{25}\eta_{24}\bar{\eta}_{14} + c_{2n}\cdots c_{26}\eta_{25}\bar{\eta}_{15}c_{14} + \cdots + \eta_{2n}\bar{\eta}_{1n}c_{1n-1}c_{1n-2}\cdots c_{14} \\
\alpha_{32} =& c_{3n}c_{3n-1}\cdots c_{35}\eta_{34}\bar{\eta}_{24} + c_{3n}\cdots c_{36}\eta_{35}\bar{\eta}_{35}c_{24} + \cdots + \eta_{3n}\bar{\eta}_{2n}c_{2n-1}c_{2n-2}\cdots c_{24} \\
\alpha_{31} =& c_{3n}c_{3n-1}\cdots c_{35}\eta_{34}\bar{\eta}_{14}c_{24} + c_{3n}\cdots c_{36}\eta_{35}c_{25}\bar{\eta}_{15}c_{14} + \cdots \\
& + \eta_{3n}c_{2n}\bar{\eta}_{1n}c_{1n-1}c_{1n-2}\cdots c_{14}.
\end{aligned} \tag{3.25}$$

Where $c_{ij} = \cos\theta_{ij}$ and $\eta_{ij} = e^{-i\phi_{ij}}\sin\theta_{ij}$.

It is important to note that while the light sector of the neutrino mixing matrix, N, is no longer unitary, the full mixing matrix, U, remains unitary.

It will be useful to define the next rectangular matrix

$$K = \begin{pmatrix} N & S \end{pmatrix}. \tag{3.26}$$

This matrix is the one that characterizes the charge current Lagrangian and we will explain it better when we talk about the non-unitary effects in the seesaw models. This matrix needs to fulfill a unitary condition

$$KK^\dagger = NN^\dagger + SS^\dagger = I. \tag{3.27}$$

We can demonstrate that the light sector of the neutrino mixing matrix is no longer unitary by computing

$$
\begin{aligned}
NN^\dagger =& N^{NP} U U^\dagger N^{NP\dagger} \\
=& \begin{pmatrix} \alpha_{11}^2 & \alpha_{11}\alpha_{21}^* & \alpha_{11}\alpha_{31}^* \\ \alpha_{11}\alpha_{21} & \alpha_{22}^2 + |\alpha_{21}|^2 & \alpha_{22}\alpha_{32}^* + \alpha_{21}\alpha_{31}^* \\ \alpha_{11}\alpha_{31} & \alpha_{22}\alpha_{32} + \alpha_{31}\alpha_{21}^* & \alpha_{33}^2 + |\alpha_{31}|^2 + |\alpha_{32}|^2 \end{pmatrix}.
\end{aligned} \tag{3.28}
$$

This modification of the mixing matrix has an impact on the oscillation probability.

We can follow the same procedure as the standard neutrino oscillation case and we can obtain the following probability

$$
\begin{aligned}
P_{\alpha\beta} = \sum_{i,j}^{3} N_{\alpha i}^* N_{\beta i} N_{\alpha j} N_{\beta j}^* - 4 \sum_{j>i}^{3} \mathrm{Re}\left[N_{\alpha j}^* N_{\beta j} N_{\alpha i} N_{\beta i}^*\right] \sin^2\left(\frac{\Delta m_{ij}^2 L}{4E_\nu}\right) \\
+ 2 \sum_{j>i}^{3} \mathrm{Im}\left[N_{\alpha j}^* N_{\beta j} N_{\alpha i} N_{\beta i}^*\right] \sin\left(\frac{\Delta m_{ij}^2 L}{2E_\nu}\right).
\end{aligned} \tag{3.29}
$$

The oscillation experiments could prove this discrepancy in the oscillation probability between the standard description and models with NHLs. The short-baseline experiments give us a perfect scenario to find constraints to the α parameters due to the zero-distance approximation. This approximation is allowed when the beam energy is bigger than the distance between the source and the detector. In this case, we can approximate $L \approx 0$ and then, the oscillation probability will be

$$
P_{\alpha\beta} = \sum_{i,j}^{3} N_{\alpha i}^* N_{\beta i} N_{\alpha j} N_{\beta j}^*. \tag{3.30}
$$

As usual, the Greek letters refer to lepton-flavor and the Latin ones denote the mass state. In this approximation, the oscillation probability only depends on the α parameters, this is easier to see using the next equivalence:

$$
N_{\alpha\beta} = \sum_{\kappa} N_{\alpha\kappa}^{NP} U_{\kappa\beta}. \tag{3.31}
$$

Then, the oscillation probabilities are [15, 17, 23]:

$$
\begin{aligned}
P_{\mu e} &= \alpha_{11}^2 |\alpha_{21}|^2, \\
P_{e\tau} &= \alpha_{11}^2 |\alpha_{31}|^2, \\
P_{\mu\tau} &\approx \alpha_{22}^2 |\alpha_{32}|^2, \\
P_{ee} &= \alpha_{11}^4, \\
P_{\mu\mu} &= (|\alpha_{21}|^2 + \alpha_{22}^2)^2, \\
P_{\tau\tau} &= (|\alpha_{31}|^2 + \alpha_{32}^2 + \alpha_{33}^2)^2.
\end{aligned} \tag{3.32}
$$

The zero-distance approximation will be useful in analyzing the FASERν and FASERν2 experiments.

3.2.1 The Degrees of Freedom of a Mixing Matrix with an Arbitrary Number of Majorana Neutrinos

We know that the whole neutrino mixing matrix must be unitary. A unitary matrix with dimension N has N^2 degrees of freedom. By looking again at Eq. (3.22), we notice that the matrix has N(N-1) parameters and we may think of the existence of a mistake in the formalism. However, this could be explained if we consider the neutrino mixing's physical parameters. We know that the NHL does not take part in the weak interaction and, for that reason, many parameters are not physical. That is the reason why we focus on counting the degrees of freedom of the rectangular matrix K, since this matrix is the one that appears in the CC Lagrangian.

Here, we are going to count the degrees of freedom for an arbitrary number of Majorana neutrinos, this computation was done in several works [21, 24]. The CC Lagrangian has $N_A = 3$ active neutrinos and an arbitrary number of massive neutrino states $N = N_A + N_S$, where N_S is the number of extra NHL. A rectangular matrix with these dimensions has $2 \times N_A \times N$ parameters, but as we know (from Eq. (3.27)) the K matrix has the property that $KK^\dagger = I_{3x3}$, then we have N_A^2 restrictions and the degrees of freedom that remains physical are $N_A(2 \times N - N_A) = N_A(2 \times N_S + N_A)$. Moreover, we know that in the case of Majorana neutrinos we can absorb 3 phases, so we expect that the K matrix in any parametrization would have $N_A(2 \times N_S + N_A - 1)$ degrees of freedom.

Besides the total number of degrees of freedom, we aim to determine the number of mixing angles and phases. To do this, we will consider a unitary matrix of size $N \times N$, which has N^2 degrees of freedom. This matrix will then be truncated to a rectangular form, to identify the remaining degrees of freedom. We will use the next $N \times N$ neutrino mixing matrix to count the degrees of freedom

$$U_{n\times n} = D(\omega)\{\prod_{a<b=1}^{N} W^{ab}(\theta_{ab}, \eta_{ab})\}, \tag{3.33}$$

where $D(\omega)_{n\times n} = diag(e^{i\omega_1} \cdots e^{i\omega_N})$ and the term between keys is the Eq.(3.22). For the $D(\omega)$ matrix, we have N degrees of freedom and the W^{ab} matrix has $N(N-1)$. The total degrees of freedom of Eq. (3.33) is N^2, as we expect.

To determine how many and which parameters are degrees of freedom, we need to truncate Eq.(3.33) to a rectangular matrix with the desired dimensions. For instance, we will consider truncating to the N_B row, where $N_B < N$. The truncated

matrix has the next form [21] [24]:

$$U_{N_B\times N} = D(\omega)_{N_B\times N_B}\left[\prod_{a=1}^{N_B}\prod_{b=1}^{N} W^{ab}(\theta_{ab},\eta_{ab})\right]_{N_B\times N}. \tag{3.34}$$

We will focus on how many parameters have the W^{ab} matrix. We count the number of indices ab allowed by the W^{ab} matrix. Using the product operator in Eq. (3.34), we found the next indices:

$$\begin{array}{cccccc} 12 & & & & & \\ 13 & 23 & & & & \\ \vdots & \vdots & \ddots & & & \\ 1N_B & 2N_B & \cdots & (N_B-1)N_B & & \\ 1(N_B+1) & 2(N_B+1) & \cdots & (N_B-1)(N_B+1) & N_B(N_B+1) & \\ \vdots & \vdots & \cdots & \vdots & \vdots & \\ 1N & 2N & \cdots & (N_B-1)N & N_BN & \end{array} \tag{3.35}$$

For each index, we have one mixing and one phase according to Eq. (3.21). We observe a triangular structure in the $(N_B-1)N_B$ index. As a result, this part contains $\frac{N_B(N_B-1)}{2}$ indices, while below this triangle, there are $N_B(N-N_B)$ indices. Then we have $N_B(N_B-1)+2N_B(N-N_B)+N_B$ degrees of freedom. The last N_B comes from the $D(\omega)_{N_B\times N_B}$ matrix. For the special case that $N_B = N_A$, which is the case that keeps our interest, we have $N_A(N_A+2\times N_S)$ degrees of freedom, as we said above. For this case, we have:

$$\frac{N_A(N_A-1)}{2} + N_AN_S = 3+3N_S \qquad mixings, \tag{3.36}$$

$$\frac{N_A(N_A+1)}{2} + N_AN_S = 6+3N_S \qquad phases. \tag{3.37}$$

As we already mentioned, we are in the Majorana neutrino case, so we can absorb 3 phases and the total amount of phases is $3+N_S$. Those three phases come from the $D(\omega)$ matrix, and all the physical parameters are in the W^{ab} matrix. We have $6+6N_S = 6\times(N-2)$ degrees of freedom, and as we remember in the symmetric parametrization (Eq. (3.21)) we have $N(N-1)$, as a consequence in our parametrization we have $N(N-1)-6(N-2) = N_S(N_S-1)$ parameters that are not observables. The parameters that are not observable are the mixing and the phases between Neutral Heavy leptons, this could be seen in the indices of ab from W^{ab} matrix, if both indices are greater than 3, the parameters are not physical. For example, mixing θ_{45} and the phase $e^{\phi_{45}}$ are not physical because it is the mixing (and phase) between two sterile neutrinos and we cannot detect it. On the other

hand, all the mixings and phases between the active and the sterile neutrinos are physical and we can observe this in the counting of the indices in Eq. (3.35). The sterile neutrinos could be indirectly detected through the active neutrinos as an anomaly in the neutrino events. An important remark is that the α parameters are described solely in terms of mixing and phases between active and sterile neutrinos. This confirms that the non-unitary parameters are physical quantities.

3.2.2 The Triangle Inequality Condition on the α Parameters

The diagonal α parameters are related to the off-diagonal ones, this happens due to the $KK^\dagger$ unitary property described in Eq.(3.27). In this subsection, we follow the computation of the triangle inequality condition from [25]:

$$\sum_{j}^{3} K_{\alpha j}K_{\beta j}^{*} + \sum_{j=4}^{n} K_{\alpha j}K_{\beta j}^{*} = \sum_{j}^{3} N_{\alpha j}N_{\beta j}^{*} + \sum_{j=1}^{n-3} S_{\alpha j}S_{\beta j}^{*} = \delta_{\alpha\beta}, \tag{3.38}$$

for the case $\alpha \neq \beta$ we have the next equivalence:

$$|\sum_{j}^{3} N_{\alpha j}N_{\beta j}^{*}|^2 = |\sum_{j=1}^{n-3} S_{\alpha j}S_{\beta j}^{*}|^2. \tag{3.39}$$

We can apply the Cauchy-Schwarz inequality to the right side of the equation above, and then use the unitary condition with $\alpha = \beta$ to get:

$$\begin{aligned} |\sum_{j}^{3} N_{\alpha j}N_{\beta j}^{*}|^2 &\leq \left(\sum_{j=1}^{n-3} |S_{\alpha j}|^2\right)\left(\sum_{j=1}^{n-3} |S_{\beta j}|^2\right) \\ &= \left(1 - \sum_{j}^{3} |N_{\alpha j}|^2\right)\left(1 - \sum_{j}^{3} |N_{\beta j}|^2\right). \end{aligned} \tag{3.40}$$

We can rewrite this inequality as:

$$|(NN^\dagger)_{\alpha\beta}|^2 \leq (1 - (NN^\dagger)_{\alpha\alpha})(1 - (NN^\dagger)_{\beta\beta}). \tag{3.41}$$

We can compute explicitly the triangle inequality in terms of the α parameters using equation (3.28). There are three triangle inequality conditions, we begin with the α_{21}:

$$\begin{aligned} |(NN^\dagger)_{e\mu}|^2 &\leq (1 - (NN^\dagger)_{ee})(1 - (NN^\dagger)_{\mu\mu}) \\ \alpha_{11}^2|\alpha_{21}|^2 &\leq (1 - \alpha_{11}^2)(1 - \alpha_{22}^2 - |\alpha_{21}|^2) \\ -\alpha_{11}^2|\alpha_{21}|^2 + |\alpha_{21}|^2 + \alpha_{11}^2|\alpha_{21}|^2 &\leq (1 - \alpha_{11}^2)(1 - \alpha_{22}^2) \\ |\alpha_{21}|^2 &\leq (1 - \alpha_{11}^2)(1 - \alpha_{22}^2). \end{aligned} \tag{3.42}$$

In the case of α_{31}, we have:

$$\begin{aligned} |(NN^\dagger)_{e\tau}|^2 &\leq (1-(NN^\dagger)_{ee})(1-(NN^\dagger)_{\tau\tau}) \\ \alpha_{11}^2|\alpha_{31}|^2 &\leq (1-\alpha_{11}^2)(1-\alpha_{33}^2-|\alpha_{31}|^2-|\alpha_{32}|^2) \\ -\alpha_{11}^2|\alpha_{31}|^2+|\alpha_{31}|^2+\alpha_{11}^2|\alpha_{31}|^2 &\leq (1-\alpha_{11}^2)(1-\alpha_{33}^2-|\alpha_{32}|^2) \\ |\alpha_{31}|^2 &\leq (1-\alpha_{11}^2)(1-\alpha_{33}^2-|\alpha_{32}|^2). \end{aligned} \tag{3.43}$$

It is straightforward to know that $(1-\alpha_{11}^2)(1-\alpha_{33}^2-|\alpha_{32}|^2) \leq (1-\alpha_{11}^2)(1-\alpha_{33}^2)$, then:

$$|\alpha_{31}|^2 \leq (1-\alpha_{11}^2)(1-\alpha_{33}^2). \tag{3.44}$$

The last triangle inequality condition is to the α_{32}

$$\begin{aligned} |(NN^\dagger)_{\mu\tau}|^2 &\leq (1-(NN^\dagger)_{\mu\mu})(1-(NN^\dagger)_{\tau\tau}), \\ |\alpha_{22}\alpha_{32}+\alpha_{21}^*\alpha_{31}|^2 &\leq (1-\alpha_{22}^2-|\alpha_{21}|^2)(1-\alpha_{33}^2-|\alpha_{31}|^2-|\alpha_{32}|^2). \end{aligned} \tag{3.45}$$

However, this case is different, we can not use the same procedure as the other two inequalities. We will focus on the terms of the left side of Eq. (3.45) and using the Cauchy-Schwarz inequality, we get:

$$|\alpha_{22}\alpha_{32}+\alpha_{21}^*\alpha_{31}|^2 \geq (\alpha_{22}|\alpha_{32}|-|\alpha_{21}||\alpha_{31}|)^2. \tag{3.46}$$

We can focus on two cases, the first one is when $\alpha_{22}|\alpha_{32}| \leq |\alpha_{21}||\alpha_{31}|$ we can use their respective inequalities (Eq. (3.42) and (3.43)) to get:

$$\begin{aligned} \alpha_{22}^2|\alpha_{32}|^2 &\leq (1-\alpha_{11}^2)^2(1-\alpha_{22}^2)(1-\alpha_{33}^2-|\alpha_{32}|^2) \\ \alpha_{22}^2|\alpha_{32}|^2 &\leq (1-\alpha_{22}^2)(1-\alpha_{33}^2-|\alpha_{32}|^2) \\ |\alpha_{32}|^2-\alpha_{22}^2|\alpha_{32}|^2+\alpha_{22}^2|\alpha_{32}|^2 &\leq (1-\alpha_{22}^2)(1-\alpha_{33}^2) \\ |\alpha_{32}|^2 &\leq (1-\alpha_{22}^2)(1-\alpha_{33}^2). \end{aligned} \tag{3.47}$$

For the case $\alpha_{22}|\alpha_{32}| \leq |\alpha_{21}||\alpha_{31}|$ we have:

$$|\alpha_{22}\alpha_{32}+\alpha_{21}^*\alpha_{31}| \geq \alpha_{22}|\alpha_{32}|-|\alpha_{21}||\alpha_{31}|. \tag{3.48}$$

Using the equation (3.45) we get:

$$\alpha_{22}|\alpha_{32}| \leq |\alpha_{21}||\alpha_{31}|\sqrt{(1-\alpha_{22}^2-|\alpha_{21}|^2)(1-\alpha_{33}^2-|\alpha_{31}|^2-|\alpha_{32}|^2)} \tag{3.49}$$

After some manipulation, we get the same form as the other cases:

$$|\alpha_{32}| = \sqrt{(1-\alpha_{33}^2)(1-\alpha_{22}^2)}. \tag{3.50}$$

In general, we can write the triangle inequality condition as:

$$\alpha_{ij} = \sqrt{(1-\alpha_{ii}^2)(1-\alpha_{jj}^2)}. \tag{3.51}$$

These inequality conditions tell us that the rectangular matrix is unitary. These conditions will be important in our numerical analysis.

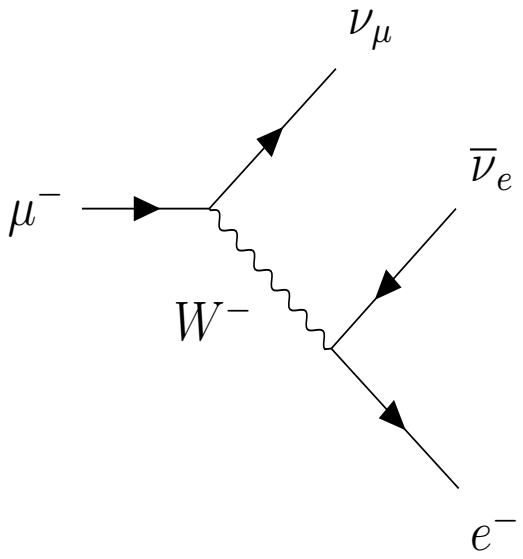

Figure 3.1: From this process comes the measurement of G_μ with the highest accuracy

3.2.3 The HNL and Electro-Weak Precision Measurements

The HNL affects the experimental observables that depend on the mixings. Our interest in this subsection is focused on the Fermi constant, G_F. This constant is measured with the highest accuracy using the process in Fig. (3.1). However, in the non-unitary case, each vertex of this process has a quadratic term of the mixing matrix and the coupling constant of this process has the next form [12, 26, 27]:

$$G_\mu = G_F \sqrt{(NN^\dagger)_{ee}(NN^\dagger)_{\mu\mu}} \tag{3.52}$$

In terms of the α parameters, we obtain:

$$G_F = \frac{G_\mu}{\sqrt{\alpha_{11}^2(\alpha_{22}^2 + |\alpha_{21}|^2)}} \tag{3.53}$$

It is important to remark that, in this scenario, G_F contains HNL effects that are valid for the particular case of the muon decay. It is for that reason that in other processes we redefine the Fermi constant through the previous equation. Other observables, like the CKM components [26], are also affected by the HNL, although that is out of the scope of this work.

3.2.4 Non-unitary Effects in Neutral Current Detection

In the case of the charge current detection, we know that the vertex of the $W^{\pm}$ is coupled to a neutrino and their corresponding charged lepton. However, in the case of the neutral current, we do not know the flavor of the final state of the neutrino. If the neutrino is generated by a charged current process then we write the probability as

$$P_{\alpha} = \sum_{\beta} P_{\alpha\beta}, \tag{3.54}$$

where the sum is over all the flavor of the final neutrino, and the α index is for the flavor of the initial neutrino. We want to compute the oscillation probability in the zero-distance approximation, so we are going to neglect the evolution of the states. A charge current process will create the initial neutrino and the detection will be through a neutral current, as we can see in Fig (3.2). Then the probability

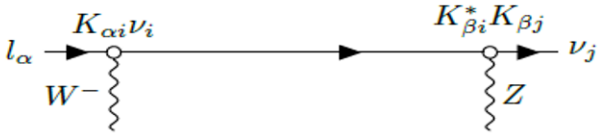

Figure 3.2: Feynman diagram of the creation and detection of the neutrino

amplitude in this process is

$$\mathcal{A}_{\alpha j} = \sum_{i,\beta}^{n,3} K_{\alpha i} K^*_{\beta i} K_{\beta j}. \tag{3.55}$$

Therefore, the probability is

$$P_{\alpha} = \sum_{i,l,j,\beta,\beta'}^{n,n,n,3,3} K_{\alpha i} K^*_{\beta i} K_{\beta j} K^*_{\beta' j} K_{\beta' l} K^*_{\alpha l}. \tag{3.56}$$

We remember that the matrix K has the property of Eq.(3.27), then we can use the equation (3.38). We use this property in the probability:

$$\begin{aligned} P_{\alpha} &= \sum_{i,l,\beta,\beta'} K_{\alpha i} K^*_{\beta i} \delta_{\beta\beta'} K_{\beta' l} K^*_{\alpha l} = \sum_{i,l,\beta} K_{\alpha i} K^*_{\beta i} K_{\beta l} K^*_{\alpha l} \\ &= \sum_{\beta} \left(\sum_{i,l}^{3} N_{\alpha i} N^*_{\beta i} N_{\beta l} N^*_{\alpha l} + \sum_{i,j>3}^{n} K_{\alpha i} K^*_{\beta i} K_{\beta l} K^*_{\alpha l} \right) \\ &= \sum_{\beta} \left(\sum_{i,l}^{3} N_{\alpha i} N^*_{\beta i} N_{\beta l} N^*_{\alpha l} + \sum_{i,j=1}^{n-3} S_{\alpha i} S^*_{\beta i} S_{\beta l} S^*_{\alpha l} \right). \end{aligned} \tag{3.57}$$

We neglect the terms of the S for its smallness

$$P_\alpha \approx \sum_{i,l,\beta}^{3} N_{\alpha i} N^*_{\beta i} N_{\beta l} N^*_{\alpha l}.$$

The probability remains the same structure as in the charged current detection case (Eq. (3.30)), with the sum over all the possible final states. Although it is not possible to determine the final flavor of a neutrino in neutral current interactions, many studies have explored the effects of non-unitarity in this context [18, 28, 29].

Chapter 4

The Seesaw Mechanism Type I and the Relation Between Different Parametrizations

After the discovery of neutrino oscillations and the realization that neutrinos have mass, several fundamental questions arose: What is the nature of the neutrino mass (Majorana or Dirac)? How do neutrinos acquire their masses, and why are these masses tiny? Various theories attempt to explain the suppression of neutrino masses by invoking the exchange of heavy fields at the tree level, such as the right-handed neutrinos in the seesaw type I [30–33], using scalar triplets as in the seesaw type II [24, 33], or using fermion triplets as in seesaw type III [34]. In this chapter, we will focus on seesaw type I because of its simplicity and rich phenomenological scheme, which is due to the low-scale seesaw type I models as the inverse and lineal seesaw.

4.1 Overview of the Seesaw Type I

In this section, we will compute the masses using the block matrix diagonalization method (BMDM) in the minimal seesaw type I, as well as in low-scale scenarios such as the linear and inverse seesaw.

4.1.1 The Most Simple and General Seesaw Type I

First, we will talk about the minimal general seesaw type I. In this scheme, we only add extra right-handed neutrinos in the SM to get tiny masses to the active neutrino. In this theory, we have the following Lagrangian mass term [35, 36]

$$\mathcal{L} = \overline{\hat{\nu}_{Li}}(M_D)_{ij}\hat{N}_{R_j} + \frac{1}{2}\overline{\hat{N}^c_{Li}}(M_R)_{ij}\hat{N}_{R_j} + h.c., \tag{4.1}$$

where $N_R^c = C\overline{N}^T$. We can describe this Lagrangian using a mass matrix

$$M_{n\times n} = \begin{pmatrix} 0_{3\times 3} & M_{D_{3\times m}} \\ M^T_{D_{m\times 3}} & M_{R_{m\times m}} \end{pmatrix}, \tag{4.2}$$

where $m = n+3$, and n is the dimension of the mass matrix, the index m represents the number of right-handed neutrinos in the theory. To obtain the mass matrix in the physical basis, we need to change the basis by performing the following transformations

$$U^T M_{n\times n} U = M_{diag}. \tag{4.3}$$

We can consider the polar decomposition to describe the matrix, U, as [37]

$$U = exp(iH)\cdot V, \tag{4.4}$$

where

$$H = \begin{pmatrix} 0 & S \\ S^\dagger & 0 \end{pmatrix}, \quad V = \begin{pmatrix} V_1 & 0 \\ 0 & V_2 \end{pmatrix}. \tag{4.5}$$

The S matrix depends on a small parameter ϵ in which we expand in power series, we get

$$\tilde{U} = \begin{pmatrix} (\mathbb{I} - \frac{1}{2}SS^\dagger)_{3\times 3} & iS_{3\times m} \\ iS^\dagger_{m\times 3} & (\mathbb{I} - \frac{1}{2}S^\dagger S)_{m\times m} \end{pmatrix} \quad V = \begin{pmatrix} V_{1_{3\times 3}} & 0 \\ 0 & V_{2_{m\times m}} \end{pmatrix}, \tag{4.6}$$

We can put equation (4.6) into (4.3) to get

$$iS^* = -M_D M_R^{-1}. \tag{4.7}$$

With this relation, we can put the mixing matrix in terms of the mass

$$\tilde{U}_{n\times n} = \begin{pmatrix} \mathbb{I}_{3\times 3} - \frac{1}{2}(M_D^*(M_R^*)^{-1}M_R^{-1}M_D^T)_{3\times 3} & (M_D^*(M_R^*)^{-1})_{3\times m}, \\ (M_R^{-1}M_D^T)_{m\times 3} & \mathbb{I}_{3\times 3} - \frac{1}{2}(M_R^{-1}M_D^T M_D^*(M_R^*)^{-1})_{m\times m} \end{pmatrix}. \tag{4.8}$$

Now, we can compute the masses in terms of the flavor basis using equation (4.8) and (4.3), at leading order, we get

$$m_{diag} = -(V_1^T(M_D M_R^{-1} M_D^T)V_1)_{3\times 3} \tag{4.9}$$

$$M_N^{diag} = (V_2^T M_R V_2)_{m\times m}. \tag{4.10}$$

This approximation, which computes the physical masses is called the BMDM.

4.1.2 The Non-Unitary Effects in the Seesaw Type I

As we said in the last chapter, the new extra neutrino massive states impact the light sector of the neutrino mixing matrix. This change will be reflected in the K matrix, which characterizes the charged current interactions. We define this matrix as [24]

$$K_{ij} = \sum_{c=1}^{n} \Omega^*_{ci} U_{cj}. \tag{4.11}$$

The Ω matrix is the charged lepton mixing matrix, and we will work on a diagonal basis, so the K matrix depends entirely on the neutrino mixing matrix. It is useful to describe this matrix as a block matrix

$$K = (N, S), \tag{4.12}$$

where N describes the mixings in the light sector and S in the sector of the new massive states. We can extract these matrices from the Eq. (4.8)

$$N = (\mathbb{I}_{3\times 3} - \frac{1}{2}(M_D^*(M_R^*)^{-1}M_R^{-1}M_D^T)_{3\times 3})V_1, \tag{4.13}$$

$$S = (M_D^*(M_R^*)^{-1})_{3\times m}V_2. \tag{4.14}$$

We can see in Eq. (4.13) that the neutrino mixing matrix deviates from the unitary matrix by a factor. This factor is the non-unitary effects in this scheme, which we can write as

$$\eta = \frac{1}{2}(M_D^*(M_R^*)^{-1}M_R^{-1}M_D^T)_{3\times 3}. \tag{4.15}$$

In the next subsection, we will discuss the non-unitary effects in the low-scale seesaw theories and find that we recover this equation in some approximations.

4.1.3 The Low-Scale Seesaw

In the minimal seesaw type I, we just add the right-handed neutrinos. However, the heavy neutrinos are in the GUT's scale, as a consequence, it is impossible to see phenomenology in the next generation of experiments. An alternative to this problem is the so-called low-scale seesaw mechanisms, which allow a reachable phenomenology in the current experiments. In the next subsection, we will talk about the inverse and the lineal seesaw.

An Overview of the Inverse Seesaw

In this model, we add an extra suppression to the neutrino mass, that is a μ matrix that must be small. In this scheme, we add right-handed neutrinos and left-handed

singlets [35, 38]. The mass matrix has the next form

$$M_\nu = \begin{pmatrix} 0 & M_D & 0 \\ M_D^T & 0 & M \\ 0 & M^T & \mu \end{pmatrix}. \tag{4.16}$$

We can compute the light masses as in the most general type I seesaw, for this reason, we can define the following matrices

$$M'_{D_{3\times 6}} = (M_{D_{3\times 3}}, 0_{3\times 3}), \quad M_{R_{6\times 6}} = \begin{pmatrix} 0_{3\times 3} & M_{3\times 3} \\ M^T_{3\times 3} & \mu_{3\times 3} \end{pmatrix}. \tag{4.17}$$

The inverse matrix of the heavy sector is:

$$M^{-1}_{R_{6\times 6}} = \begin{pmatrix} -((M^T)^{-1}\mu M^{-1})_{3\times 3} & (M)^{-1}_{3\times 3} \\ (M^T)^{-1}_{3\times 3} & 0 \end{pmatrix}. \tag{4.18}$$

We can compute the m_ν the same way as in Eq. (4.9), using the equation (4.3), we get the next equation

$$m_{\nu_{3\times 3}} = (M_D(M^T)^{-1}\mu M^{-1} M_D^T)_{3\times 3}, \quad M_{N_{6\times 6}} = M_{R_{6\times 6}}. \tag{4.19}$$

In this case, using the equations (4.6) and (4.3), we can find the S matrix

$$\begin{aligned} iS^* &= -M'_{D_{3\times 6}} M^{-1}_{R_{6\times 6}} \\ &= -(M_{D_{3\times 3}}, 0_{3\times 3}) \cdot \begin{pmatrix} -((M^T)^{-1}\mu M^{-1})_{3\times 3} & (M)^{-1}_{3\times 3} \\ (M^T)^{-1}_{3\times 3} & 0 \end{pmatrix} \\ &= ((M_D(M^T)^{-1}\mu M^{-1})_{3\times 3}, -(M_D M^{-1})_{3\times 3}). \end{aligned} \tag{4.20}$$

In the limit $\mu \longrightarrow 0$ we have:

$$iS^* = (0_{3\times 3}, -(M_D M^{-1})_{3\times 3}). \tag{4.21}$$

Using equation (4.21) into (4.6) we can write the non-unitary deviation in this model:

$$\eta = \frac{1}{2}(M_D^*(M_R^*)^{-1} M_R^{-1} M_D^T)_{3\times 3} \tag{4.22}$$

and we recover Eq. (4.15).

An Overview of the Linear Seesaw

Another low-scale model to try to explain the neutrino mass is the Linear seesaw mechanism [39]. The linear seesaw avoids the μ term, instead, the second suppression

comes from M_L. However, in this work, we are not interested in the model building that allows these low-scale models, but in the rich phenomenology that we can study. In this scheme, the mass matrix is

$$M_\nu = \begin{pmatrix} 0 & M_D & M_L \\ M_D^T & 0 & M \\ M_L^T & M^T & 0 \end{pmatrix}. \tag{4.23}$$

In the same way that in the inverse seesaw, we can define the following block matrices

$$M'_{DL_{3\times 6}} = (M_{D_{3\times 3}}, M_{L_{3\times 3}}), \quad M^L_{R_{6\times 6}} = \begin{pmatrix} 0_{3\times 3} & M_{3\times 3} \\ M^T_{3\times 3} & 0 \end{pmatrix}. \tag{4.24}$$

The inverse matrix of the heavy sector is

$$M^{L^{-1}}_{R_{6\times 6}} = \begin{pmatrix} 0_{3\times} & (M^T)^{-1}_{3\times 3} \\ (M)^{-1}_{3\times 3} & 0_{3\times 3} \end{pmatrix}. \tag{4.25}$$

We can use the equation (4.6) and (4.8) to get a relation between the S matrix and the mass matrix, we find that is the same relation as the other schemes

$$\begin{aligned} iS^* &= -M'_{DL_{3\times 6}} M^{L^{-1}}_{R_{6\times 6}} \\ &= -(M_{D_{3\times 3}}, M_{L_{3\times 3}}) \cdot \begin{pmatrix} 0_{3\times 3} & (M)^{-1}_{3\times 3} \\ (M^T)^{-1}_{3\times 3} & 0 \end{pmatrix} \\ &= -(M_L(M^{-1})_{3\times 3}, (M_D M^{-1})_{3\times 3}), \end{aligned} \tag{4.26}$$

the neutrino masses are

$$m_{\nu_{3\times 3}} = M_D(M_L M^{-1})^T + (M_L M^{-1}) M_D^T, \quad M_{N_{6\times 6}} = M_{R_{6\times 6}}. \tag{4.27}$$

In the limit $M_L \longrightarrow 0$,

$$N = (\mathbb{I}_{3\times 3} - \eta^{LS}_{3\times 3}) \cdot V_{1_{3\times 3}}, \quad S = (0_{3\times 3}, (M_D^*(M^{*T})^{-1})_{3\times 3}) \cdot V_{2_{6\times 6}}, \tag{4.28}$$

and the non-unitary effects are characterized by:

$$\eta^{LS} = \frac{1}{2}(M_D^*(M^*)^{-1} M^{-1} M_D^T)_{3\times 3}. \tag{4.29}$$

We have some limits where the three models have the same nonunitary effects.

4.2 The Symmetric Parametrization in the Linear Seesaw Models

As we said in the last chapter, symmetric parametrization is used to constrain the non-unitary parameters in oscillation experiments. An important feature is that this parametrization is model-independent. For this reason, we need to see how the parametrization works in the seesaw model. We will begin with the simplest case, with only three extra right-handed neutrinos. We can compute the neutrino mixing matrix using equation (3.22), for this case we get [40–42]:

$$U = \omega_{56}\omega_{46}\omega_{36}\omega_{26}\omega_{16}\omega_{45}\omega_{35}\omega_{25}\omega_{15}\omega_{34}\omega_{24}\omega_{14}\omega_{23}\omega_{13}\omega_{12} \tag{4.30}$$

$$= U^{NHL}U^{3\times3}, \tag{4.31}$$

where,

$$U^{NHL} = \omega_{56}\omega_{46}\omega_{36}\omega_{26}\omega_{16}\omega_{45}\omega_{35}\omega_{25}\omega_{15}\omega_{34}\omega_{24}\omega_{14}. \tag{4.32}$$

The ω matrices related to heavy mixings commute with the ω matrices related to mixing between heavy and light states. We can rearrange the equation above as

$$U^{NHL} = \omega_{56}\omega_{46}\omega_{45}\omega_{36}\omega_{26}\omega_{16}\omega_{35}\omega_{25}\omega_{15}\omega_{34}\omega_{24}\omega_{14}. \tag{4.33}$$

We can notice that the matrices that mix the heavy sector are now grouped[42]:

$$U^{H} = \omega_{56}\omega_{46}\omega_{45}. \tag{4.34}$$

All the information about the new physical parameters is contained in the term

$$U^{LH} = \omega_{36}\omega_{26}\omega_{16}\omega_{35}\omega_{25}\omega_{15}\omega_{34}\omega_{24}\omega_{14}. \tag{4.35}$$

The full mixing matrix in this case is

$$U_{6\times6} = U^{H}U^{LH}U^{3\times3} = \begin{pmatrix} I_{3\times3} & 0_{3\times3} \\ 0_{3\times3} & \omega_{56}\omega_{46}\omega_{45} = H_{3\times3} \end{pmatrix} U^{LH} \begin{pmatrix} U^{PMNS} & 0_{3\times3} \\ 0_{3\times3} & I_{3\times3} \end{pmatrix}, \tag{4.36}$$

where $H_{3\times3}$ is the unitary matrix that diagonalizes the heavy sector. In this sense, it is somehow analog to the U^{PMNS}, which is a unitary mixing matrix for the light sector. The U^{PMNS} is composed by $(\omega_{23}\omega_{13}\omega_{12})$. We want to see if this parametrization gives us the same results as in Eqs. (4.9), (4.19), and (4.27). We work under the hypothesis that the mixings between active and sterile neutrinos are small. Therefore, we retain only the quadratic terms in the power series expansions of the sine and cosine functions, as in the case of the S element in the polar decomposition of Eq. (4.6). The ω matrix has the next form

$$\omega_{13} = \begin{pmatrix} 1 - \frac{1}{2}\theta_{13}^2 & 0 & \hat{\theta}_{13}^{*} \\ 0 & 1 & 0 \\ -\hat{\theta}_{13} & 0 & 1 - \frac{1}{2}\theta_{13}^2 \end{pmatrix}, \tag{4.37}$$

where $\hat{\theta}_{ij} = \theta_{ij}e^{i\phi_{ij}}$. The light sector of the U^{LH}, after the expansion, is

$$U_L^{LH} \approx I_{3\times3} - \begin{pmatrix} \frac{1}{2}(\theta_{14}^2+\theta_{15}^2+\theta_{16}^2) & 0 & 0 \\ \hat{\theta}_{16}\hat{\theta}_{26}^* + \hat{\theta}_{15}\hat{\theta}_{25}^* + \hat{\theta}_{14}\hat{\theta}_{24}^* & \frac{1}{2}(\theta_{24}^2+\theta_{25}^2+\theta_{26}^2) & 0 \\ \hat{\theta}_{16}\hat{\theta}_{36}^* + \hat{\theta}_{15}\hat{\theta}_{35}^* + \hat{\theta}_{14}\hat{\theta}_{34}^* & \hat{\theta}_{26}\hat{\theta}_{36}^* + \hat{\theta}_{25}\hat{\theta}_{35}^* + \hat{\theta}_{24}\hat{\theta}_{34}^* & \frac{1}{2}(\theta_{14}^2+\theta_{15}^2+\theta_{16}^2) \end{pmatrix}. \tag{4.38}$$

The deviation from the identity will be called α' matrix. We can generalize this result to an arbitrary number of new neutral heavy leptons as follows:

$$\alpha' = \begin{pmatrix} \sum_{j=4}^{n} \frac{1}{2}(\theta_{1j}^2) & 0 & 0 \\ \sum_{j=4}^{n} \hat{\theta}_{1j}\hat{\theta}_{2j}^* & \sum_{j=4}^{n} \frac{1}{2}(\theta_{2j}^2) & 0 \\ \sum_{j=4}^{n} \hat{\theta}_{1j}\hat{\theta}_{3j}^* & \sum_{j=4}^{n} \hat{\theta}_{2j}\hat{\theta}_{3j}^* & \sum_{j=4}^{n} \frac{1}{2}(\theta_{3j}^2) \end{pmatrix}, \tag{4.39}$$

where n is the total number of neutral leptons. We can see that adding more neutral heavy leptons adds mixing angles to the α'. We now need to determine the whole matrix U^{LH} to compute the light masses and prove that are the same as described in the last section. We can parametrize the U^{LH} as:

$$U^{LH} = \begin{pmatrix} U'_{L_{3\times3}} & S_{3\times3} \\ -S_{3\times3}^{\dagger} & V_{3\times3} \end{pmatrix}. \tag{4.40}$$

In terms of the mixing angles, the matrix S takes the next form

$$S_{3\times3} = \begin{pmatrix} \hat{\theta}_{14}^* & \hat{\theta}_{15}^* & \hat{\theta}_{16}^* \\ \hat{\theta}_{24}^* & \hat{\theta}_{25}^* & \hat{\theta}_{26}^* \\ \hat{\theta}_{34}^* & \hat{\theta}_{35}^* & \hat{\theta}_{36}^* \end{pmatrix}, \tag{4.41}$$

for more neutral heavy lepton states we add more columns with the same pattern:

$$S_{3\times j} = \begin{pmatrix} \hat{\theta}_{14}^* & \hat{\theta}_{15}^* & \hat{\theta}_{16}^* & \cdots & \hat{\theta}_{1j}^* \\ \hat{\theta}_{24}^* & \hat{\theta}_{25}^* & \hat{\theta}_{26}^* & \cdots & \hat{\theta}_{2j}^* \\ \hat{\theta}_{34}^* & \hat{\theta}_{35}^* & \hat{\theta}_{36}^* & \cdots & \hat{\theta}_{3j}^* \end{pmatrix}. \tag{4.42}$$

As we see the S matrix, in general, is rectangular and the case of 3 extra NHLs is the only case where the matrix is squared. The V matrix in terms of the mixing angles for the case of 3 extra NHLs is

$$V_{3\times3} = \begin{pmatrix} 1-\frac{1}{2}(\theta_{14}^2+\theta_{24}^2+\theta_{34}^2) & 0 & 0 \\ -\hat{\theta}_{15}\hat{\theta}_{14}^* - \hat{\theta}_{25}\hat{\theta}_{24}^* - \hat{\theta}_{35}\hat{\theta}_{34}^* & 1-\frac{1}{2}(\theta_{15}^2+\theta_{25}^2+\theta_{35}^2) & 0 \\ -\hat{\theta}_{16}\hat{\theta}_{14}^* - \hat{\theta}_{26}\hat{\theta}_{24}^* - \hat{\theta}_{36}\hat{\theta}_{34}^* & -\hat{\theta}_{16}\hat{\theta}_{15}^* - \hat{\theta}_{26}\hat{\theta}_{25}^* - \hat{\theta}_{36}\hat{\theta}_{35}^* & 1-\frac{1}{2}(\theta_{16}^2+\theta_{26}^2+\theta_{36}^2) \end{pmatrix}, \tag{4.43}$$

For an arbitrary number of new states, the matrix has a dimension $m \times m$ and is given by

$$V_{m\times m} = \begin{pmatrix} 1-\sum_{i=1}^{3}\frac{1}{2}(\theta_{i4}^2) & 0 & 0 & \cdots & 0 \\ -\sum_{i=1}^{3}\hat{\theta}_{i5}\hat{\theta}_{i4}^* & 1-\sum_{i=1}^{3}\frac{1}{2}(\theta_{i5}^2) & 0 & \cdots & 0 \\ -\sum_{i=1}^{3}\hat{\theta}_{i6}\hat{\theta}_{i4}^* & -\sum_{i=1}^{3}\hat{\theta}_{i6}\hat{\theta}_{i5}^* & 1-\sum_{i=1}^{3}\frac{1}{2}(\theta_{i6}^2) & \cdots & 0 \\ \vdots & \vdots & \vdots & \ddots & \vdots \\ -\sum_{i=1}^{3}\hat{\theta}_{im}\hat{\theta}_{i4}^* & -\sum_{i=1}^{3}\hat{\theta}_{im}\hat{\theta}_{i5}^* & -\sum_{i=1}^{3}\hat{\theta}_{im}\hat{\theta}_{i6}^* & \cdots & \sum_{i=1}^{3}\frac{1}{2}(\theta_{im}^2) \end{pmatrix}. \tag{4.44}$$

With this structure of the matrices, we can compute equation (4.3) using the equation (4.36). To compute the masses, first, we need to define the mixing matrix with the new parametrization

$$U_{6\times 6} = \begin{pmatrix} U_L^{LH}U_{3\times 3}^{PMNS} & S_{3\times 3} \\ -HS^{\dagger}U_{3\times 3}^{PMNS} & HV_{3\times 3} \end{pmatrix}. \tag{4.45}$$

To diagonalize the mass matrix, we need the transpose of the matrix above

$$U_{6\times 6}^{T} = \begin{pmatrix} U^{PMNS^T}U_{L_{3\times 3}}^{LH^T} & -U^{PMNS^T}S^*H_{3\times 3}^T \\ S^T & V^TH_{3\times 3}^T \end{pmatrix}. \tag{4.46}$$

It is important to remember that we can rewrite the matrices U_L^{LH} and V as:

$$U_{L_{3\times 3}}^{LH} = I_{3\times 3} - \delta_{3\times 3} \qquad \delta_{3\times 3} \sim \mathcal{O}(\theta_{\mathrm{ij}}^2), \tag{4.47}$$

$$V_{3\times 3} = I_{3\times 3} - \Delta_{3\times 3} \qquad \Delta_{3\times 3} \sim \mathcal{O}(\theta_{\mathrm{ij}}^2). \tag{4.48}$$

Then, we can compute the equation (4.3) using the mass matrix of equation (4.65)

$$\begin{aligned} U^TM_\nu U_{11} =& -U^{PMNS^T}(I-\delta)^TM_DHS^{\dagger}U^{PMNS} - U^{PMNS^T}S^*H^TM_D^T(I-\delta)U^{PMNS} \\ &+ U^{PMNS^T}S^*H^TM_RHS^{\dagger}U^{PMNS}, \end{aligned} \tag{4.49}$$

$$\begin{aligned} U^TM_\nu U_{12} =& U^{PMNS^T}(I-\delta)^TM_DH(I_{3\times 3}-\Delta_{3\times 3}) - U^{PMNS^T}S^*H^TM_D^TS \\ &- U^{PMNS^T}S^*H^TM_RH(I_{3\times 3}-\Delta_{3\times 3}), \end{aligned} \tag{4.50}$$

$$\begin{aligned} U^TM_\nu U_{21} =& -S^TM_DHS^{\dagger}U^{PMNS} + V^TH^TM_D^T(I_{3\times 3}-\delta_{3\times 3})U^{PMNS} \\ &- (I_{3\times 3}-\Delta_{3\times 3})^TH^TM_RHS^{\dagger}U^{PMNS}, \end{aligned} \tag{4.51}$$

$$\begin{aligned} U^TM_\nu U_{22} =& S^TM_DH(I_{3\times 3}-\Delta_{3\times 3})^T + (I_{3\times 3}-\Delta_{3\times 3})^TH^TM_D^TS \\ &+ (I_{3\times 3}-\Delta_{3\times 3})^TH^TM_RH(I_{3\times 3}-\Delta_{3\times 3}). \end{aligned} \tag{4.52}$$

The $U^TM_\nu U_{12}$ and U^TMU_{21} are zero because this matrix is in the mass basis, at leading order in θ_{ij} we have:

$$\begin{aligned} U^TMU_{12} &\approx U^{PMNS^T}M_DH - U^{PMNS^T}S^*H^TM_RH = 0, \\ S^*H^T &= M_DM_R^{-1}. \end{aligned} \tag{4.53}$$

The equation above matches the mixing angles of the new extra states with the mass matrix of the model. Now, we can compute the physical masses using equations (4.49) and (4.52). First, we compute the light masses at the leading order of θ_{ij}:

$$\begin{aligned} U^T M U_{11} \approx & - U^{PMNS^T} M_D H S^\dagger U^{PMNS} - U^{PMNS^T} S^* H^T M_D^T U^{PMNS} \\ & + U^{PMNS^T} S^* H^T M_R H S^\dagger U^{PMNS} = m_{diag}. \end{aligned} \tag{4.54}$$

We use equation (4.53) in (4.54):

$$\begin{aligned} & - U^{PMNS^T} M_D M_R^{-1} M_D^T U^{PMNS} - U^{PMNS^T} M_D M_R^{-1} M_D^T U^{PMNS} \\ & + U^{PMNS^T} M_D M_R^{-1} M_R M_R^{-1} M_D^T U^{PMNS} = -U^{PMNS^T} M_D M_R^{-1} M_D^T U^{PMNS}. \end{aligned}$$

Then, we have

$$m_{diag} = -U^{PMNS^T} M_D M_R^{-1} M_D^T U^{PMNS}. \tag{4.55}$$

We recover the mass of the most simple realization of the seesaw type I $m_\nu = -M_D M_R^{-1} M_D^T$. Also, we can see that the U^{PMNS} diagonalizes the light sector, as the V_1 matrix did in the last section. We show that this parametrization of the mixing matrix recovers the light masses of the simplest seesaw type I, now we compute the masses of the heavy sector using equation (4.52) at leading order:

$$\begin{aligned} U^T M_\nu U_{22} \approx & S^T M_D H + H^T M_D^T S + H^T M_R H - \Delta_{3\times3}^T H^T M_R H - H^T M_R H \\ & - H^T M_R H \Delta_{3\times3}. \end{aligned} \tag{4.56}$$

We keep the only term that is at zeroth order:

$$U^T M_\nu U_{22} \approx H^T M_R H = M_{diag}. \tag{4.57}$$

We recover the mass of the heavy sector and we see that the matrix H is the matrix that diagonalizes the heavy sector, in analogy with the V_2 matrix. It is time to do the same with low-scale seesaw models. As we said above, this parametrization is model-independent, in other words, it does not matter the structure of the mass matrix only matter how many new NHL states are in the theory. For this reason, using models with 6 extra NHLs, as the inverse and linear seesaw, leads to the same mixing matrix in the symmetric parameterization

$$U_{9\times9} = \begin{pmatrix} I_{3\times3} & 0_{3\times6} \\ 0_{6\times3} & H_{6\times6} \end{pmatrix} U_{9\times9}^{LH} \begin{pmatrix} U_{3\times3}^{PMNS} & 0_{3\times6} \\ 0_{6\times3} & I_{6\times6} \end{pmatrix}. \tag{4.58}$$

Some works with a similar approach are done in the literature [43].

In the inverse and linear seesaw cases, the matrix H is:

$$H_{6\times6} = \omega_{89}\omega_{79}\omega_{69}\omega_{59}\omega_{49}\omega_{78}\omega_{68}\omega_{58}\omega_{48}\omega_{67}\omega_{57}\omega_{47}\omega_{56}\omega_{46}\omega_{45}. \tag{4.59}$$

It is important to remember that all the ω matrices, in this case, are dimension 9×9. However, it only acts in the submatrix 6×6 that we call the H matrix. In this case, $U^{LH}_{9\times 9}$ is:

$$U^{LH} = \omega_{39}\omega_{29}\omega_{19}\omega_{38}\omega_{28}\omega_{18}\omega_{37}\omega_{27}\omega_{17}\omega_{36}\omega_{26}\omega_{16}\omega_{35}\omega_{25}\omega_{15}\omega_{34}\omega_{24}\omega_{14}. \tag{4.60}$$

We focus now on the inverse seesaw case. It would be important to rewrite the mass matrix as a matrix with 4 submatrices to get the same form that we used in the minimal seesaw type I. With this in mind, we will use equation (4.17) to obtain

$$M_{9\times 9} = \begin{pmatrix} 0_{3\times 3} & M'_{D_{3\times 6}} \\ M'^{T}_{D_{6\times 3}} & M'_{R_{6\times 6}} \end{pmatrix}, \tag{4.61}$$

in this case, we can parametrize the U^{LH} matrix as

$$U^{LH}_{9\times 9} = \begin{pmatrix} U'_L U^{PMNS}_{3\times 3} & S_{3\times 6} \\ -(HS^{\dagger}U^{PMNS})_{6\times 3} & HV_{6\times 6} \end{pmatrix}. \tag{4.62}$$

We can express the submatrices in terms of the mixing angles using Eqs. (4.39), (4.42) and (4.44). We can do the same procedure to compute the Eq. (4.3) and we obtain the same Eqs. (4.49-4.52) with the only difference being the dimension of the matrices. The matrix M_R has different scales because the μ matrix commonly is smaller than the M matrix. We can compute the Eq. (4.53) for this case and get

$$\begin{aligned} S^{*}_{3\times 6}H^{T}_{6\times 6} = M'_{D_{3\times 6}}M'^{-1}_{R_{6\times 6}} &= (M_{D_{3\times 3}}, 0_{3\times 3}) \begin{pmatrix} -((M^T)^{-1}\mu M^{-1})_{3\times 3} & (M^T)^{-1}_{3\times 3} \\ (M)^{-1}_{3\times 3} & 0 \end{pmatrix} \\ &= (-M_{D_{3\times 3}}((M^T)^{-1}\mu M^{-1})_{3\times 3}, M_{D_{3\times 3}}(M^T)^{-1}_{3\times 3}). \end{aligned} \tag{4.63}$$

We know the form of the S matrix, and we can compute the light masses using the

Eq. (4.54):

$$
\begin{aligned}
&U^T M_\nu U_{11} \approx \\
&- U^{PMNS^T} \begin{pmatrix} M_{D_{3\times3}} & 0_{3\times3} \end{pmatrix} \begin{bmatrix} -(M^T)^{-1}_{3\times3}\mu_{3\times3}M^{-1}_{3\times3}M^T_{D_{3\times3}} \\ (M)^{-1}_{3\times3}M^T_{D_{3\times3}} \end{bmatrix} U^{PMNS} \\
&- U^{PMNS^T}(-M_{D_{3\times3}}((M^T)^{-1}\mu M^{-1})_{3\times3}, M_{D_{3\times3}}(M^T)^{-1}_{3\times3}) \begin{bmatrix} M^T_{D_{3\times3}} \\ 0_{3\times3} \end{bmatrix} U^{PMNS} \\
&+ U^{PMNS^T} \begin{pmatrix} -M_{D_{3\times3}}((M^T)^{-1}\mu M^{-1})_{3\times3} & M_{D_{3\times3}}(M^T)^{-1}_{3\times3}) \end{pmatrix} \begin{pmatrix} 0_{3\times3} & M_{3\times3} \\ M^T_{3\times3} & \mu_{3\times3} \end{pmatrix} \\
&\times \begin{bmatrix} -(M)^{-1}_{3\times3}\mu_{3\times3}M^{-1}_{3\times3}M^T_{D_{3\times3}} \\ (M^T)^{-1}_{3\times3}M^T_{D_{3\times3}} \end{bmatrix} U^{PMNS} \\
&= U^{PMNS^T} M_{D_{3\times3}}(M^T)^{-1}_{3\times3}\mu_{3\times3}M^{-1}_{3\times3}M^T_{D_{3\times3}} U^{PMNS} \\
&+ U^{PMNS^T} M_{D_{3\times3}}(M^T)^{-1}_{3\times3}\mu_{3\times3}M^{-1}_{3\times3}M^T_{D_{3\times3}} U^{PMNS} \\
&- U^{PMNS^T} M_{D_{3\times3}}(M^T)^{-1}_{3\times3}\mu_{3\times3}M^{-1}_{3\times3}M^T_{D_{3\times3}} U^{PMNS} \\
&= U^{PMNS^T} M_{D_{3\times3}}(M^T)^{-1}_{3\times3}\mu_{3\times3}M^{-1}_{3\times3}M^T_{D_{3\times3}} U^{PMNS} = m_{diag}.
\end{aligned} \tag{4.64}
$$

We recover the equation (4.19), and as the last case the U^{PMNS} matrix diagonalizes the light sector. In the case of heavy masses, we do not need to compute again, we keep the zeroth order term of the equation (4.57) $M_{diag_{6\times6}} = H^T M'_R H$.

This form of the heavy masses remains for the linear seesaw model with the difference that the M_R has other structure. In fact, in the case of the linear seesaw model, we use the same mixing matrix as the inverse model, but with a different mass matrix that is defined by the equation (4.24):

$$
M_{9\times9} = \begin{pmatrix} 0_{3\times3} & M'_{DL_{3\times6}} \\ M'^T_{DL_{6\times3}} & M^L_{R_{6\times6}} \end{pmatrix}. \tag{4.65}
$$

As in the other cases, we want a relation between the model's mixing angles and the mass matrices. For the reason above, we want to get the expression for Eq. (4.53)

$$
\begin{aligned}
S^*_{3\times6}H^T_{6\times6} = M'_{DL_{3\times6}}M^{L^{-1}}_{R_{6\times6}} &= \begin{pmatrix} M_{D_{3\times3}} & M_{L_{3\times3}} \end{pmatrix} \begin{pmatrix} 0_{3\times} & (M^T)^{-1}_{3\times3} \\ (M)^{-1}_{3\times3} & 0_{3\times3} \end{pmatrix} \\
&= \begin{pmatrix} M_{L_{3\times3}}(M)^{-1}_{3\times3} & M_{D_{3\times3}}(M^T)^{-1}_{3\times3}) \end{pmatrix}.
\end{aligned} \tag{4.66}
$$

With this result, we can get the masses of the light sector using the equation (4.49)

$$
\begin{aligned}
&U^T M_\nu U_{11} \approx \\
&- U^{PMNS^T} \begin{pmatrix} M_{D_{3\times3}} & M_{L_{3\times3}} \end{pmatrix} \begin{bmatrix} (M^{-1})^T_{3\times3} M^T_{L_{3\times3}} \\ (M)^{-1}_{3\times3} M^T_{D_{3\times3}} \end{bmatrix} U^{PMNS} \\
&- U^{PMNS^T} \begin{pmatrix} M_{L_{3\times3}}(M)^{-1}_{3\times3} & M_{D_{3\times3}}(M^T)^{-1}_{3\times3} \end{pmatrix} \begin{bmatrix} M^T_{D_{3\times3}} \\ M^T_{L_{3\times3}} \end{bmatrix} U^{PMNS} \\
&+ U^{PMNS^T} \begin{pmatrix} M_{L_{3\times3}}(M)^{-1}_{3\times3} & M_{D_{3\times3}}(M^T)^{-1}_{3\times3} \end{pmatrix} \begin{pmatrix} 0_{3\times3} & M_{3\times3} \\ M^T_{3\times3} & 0_{3\times3} \end{pmatrix} \\
&\times \begin{bmatrix} (M^{-1})^T_{3\times3} M^T_{L_{3\times3}} \\ (M)^{-1}_{3\times3} M^T_{D_{3\times3}} \end{bmatrix} U^{PMNS} \\
&= -U^{PMNS^T}(M_D(M_L M^{-1})^T + (M_L M^{-1})M_D^T)U^{PMNS} \\
&- U^{PMNS^T}(M_D(M_L M^{-1})^T + (M_L M^{-1})M_D^T)U^{PMNS} \\
&+ U^{PMNS^T}(M_D(M_L M^{-1})^T + (M_L M^{-1})M_D^T)U^{PMNS} \\
&= -U^{PMNS^T}(M_D(M_L M^{-1})^T + (M_L M^{-1})M_D^T)U^{PMNS} = m_{diag}.
\end{aligned} \tag{4.67}
$$

We recover the linear seesaw's light masses as described in the last section. We reproduce all the masses of the three models using another parametrization for the mixing matrix. In this case, it has more physical meaning than the other parametrization. In the symmetric parametrization, the small parameter is the mixing angle between the active and the heavy states. We observe a correspondence between the two parameterizations, as both yield the same results on the mass basis. Consequently, we expect the non-unitary description to exhibit this correspondence. For the polar decomposition of the mixing matrix, we have the η matrix that describes the non-unitary effects and for the symmetric parametrization, we have the α' matrix. Both parameterizations must describe the same way neutrino oscillation, with this in mind, we will use the Eqs. (4.13) and (4.39) to get an equivalence between these parametrizations:

$$(I - \eta)U^{PDG} = (I - \alpha')U^{sym}, \tag{4.68}$$

where U^{PDG} is the PDG parametrization of the neutrino mixing matrix and U^{sym} is the active mixing matrix in the symmetric parametrization. Both sides of the equation are an approximation to second order in their respective parameters (for the η parametrization the parameter is $M_D M_R^{-1}$ and for the symmetric one is θ_{iN}, where N refers to the heavy states). The match between the η and α' using the equation (4.68) seems straightforward. However, this presents some issues because the mixing matrix is not the same in both parametrizations. We are only interested in the equivalence of the non-unitary effects so we can skip this problem by multiplying

the neutrino mixing with their conjugate matrix

$$NN^\dagger = (\mathbb{I} - \eta)(\mathbb{I} - \eta)^\dagger = \mathbb{I} - 2\eta + \mathcal{O}(2) \tag{4.69}$$

$$NN^\dagger = (\mathbb{I} - \alpha')(\mathbb{I} - \alpha')^\dagger = \mathbb{I} - (\alpha' + \alpha'^\dagger) + \mathcal{O}(2) \tag{4.70}$$

$$\eta = \frac{1}{2}(\alpha' + \alpha'^\dagger) = \frac{1}{2}\begin{pmatrix} 2\alpha'_{11} & \alpha'^*_{21} & \alpha'^*_{31} \\ \alpha'_{21} & 2\alpha'_{22} & \alpha'^*_{32} \\ \alpha'_{31} & \alpha'_{32} & 2\alpha'_{33} \end{pmatrix}. \tag{4.71}$$

The equation above shows a relationship between the two parametrizations that describe the non-unitary effects. This will be important in our work because we can use the current limits of the non-unitary parameters that came from neutrino experiments and use it to constrain an observable that is related to the seesaw mechanism.

Chapter 5

The Non-Unitary Effects in the FASERν Detector and a Forecast to FASERν2

The FASERν detector will be a great laboratory to study the deviation of the neutrino mixing matrix due to their high statistics in the neutrino and antineutrino events. Recently, the FASER Collaboration reported their first neutrino detection [44]. With this breakthrough, we now have a new source of neutrinos that could provide valuable insights and potential evidence of new physics in the neutrino sector. In this chapter, we will discuss the FASER experiment and the FASERν detector, the neutrino event computation, the non-unitary analysis, and a forecast for the second phase of the FASER ν2 detector.

5.1 The FASER Experiment and the FASERν Detector, a Brief Description

The main goal of The ForwArd Search ExpeRiment (FASER) is to search very weakly interacting particles in the LHC; these particles travel long distances through concrete and rock without interaction and then decay into visible particles in the detector decay volume [45]. The weakly interacting particle candidates include neutral heavy leptons (NHLs), light gauge bosons, and axion-like particles, among others. We will focus on the subdetector called FASERν; this subdetector was created to take advantage of the great number of neutrinos that are produced in the LHC collisions via hadron decays. The FASERν detector consist of a 1.2 tons Tungsten target and has a 480 m baseline. It works in an energy regime from 100 GeV to 1 TeV, and the detection will be through CC interaction.

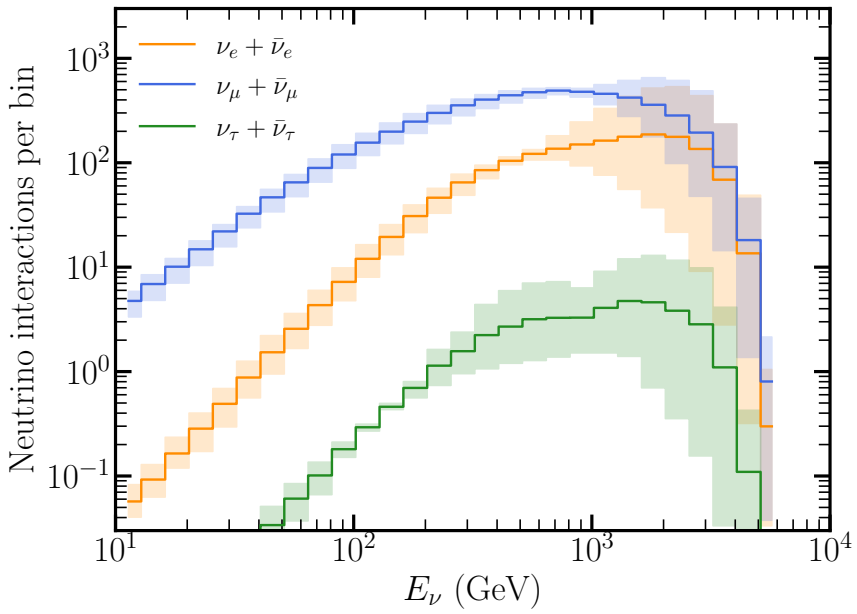

Figure 5.1: Neutrino interactions per bin vs the neutrino energy at the FASERν detector with 150 fb^{-1} integrated luminosity, according to Ref. [47].

5.2 Computing the Neutrino Events Number

Although the FASER collaboration has computed the interaction at the FASERν detector [46], there is recent work with more accuracy in the neutrino events and the uncertainties using various event generators [47]. We use this data to recompute the number of events using the next equation

$$N_\alpha^{SM} = \epsilon_\alpha N_T \int f(E_{reco}) R(E_{reco}, E_\nu) \sigma_\alpha(E_\nu) \phi_\alpha dE_\nu dE_{reco}, \tag{5.1}$$

where σ_α is the neutrino-nucleus DIS cross section, ϕ_α is the expected flux at the detector, $R(E_{reco}, E_\nu)$ is the gaussian smearing function of width $0.3E_\nu$, N_T is the number of targets in the experiment, $f(E_{reco})$ is the vertex reconstruction efficiency and ϵ_α is the charged-lepton identification efficiency ($\epsilon_e = 100\%$,$\epsilon_\mu = 86\%$,$\epsilon_\tau = 76\%$).
In Fig. 5.1, we reproduce the neutrino interaction rates per bin as reported by [47]. Using Eq. (5.1), we will also compute the expected number of events for FASERν2. FASERν2 is an upgrade of the current detector at LHC with a target mass of 20 tonnes and 20 times the luminosity. Consequently, FASERν2 will have two orders of magnitude more events than the previous detector. For FASERν, we compute the neutrino events into different cases; the first case uses all of the energy range of Fig. 5.1. The second case uses an energy region smaller than the first case to avoid

	FASERν		FASERν2	
Lepton flavor	$10^2 - 10^4$ GeV	$100 - 600$ GeV	$10^2 - 10^4$ GeV	$100 - 600$ GeV
e	1095±937	307±101	44230	20775
μ	2807±909	1163±190	193630	85044
τ	19±19	6±4	767	314

Table 5.1: Expected number of events with their corresponding systematic uncertainties used in the analysis, for the different cases. For the forecast of FASERν2, we will consider two systematic uncertainties, 5% and 10%, in accordance with [23] .

the big uncertainties in the high-energy regime; this region is between 100-600 GeV. As a consequence, we have fewer neutrino events, but at the same time, we have smaller systematical uncertainties that could help in the analysis. For FASERν2, we consider two cases; the first is with 5% of systematical uncertainty, and the second is with 10%. We can see the neutrino events in Table 5.1.

5.3 The χ^2 Analysis

We want the expected sensitivity of the non-unitary parameters through a χ^2 analysis, but first, we need to talk about the approximation that we will make for the non-unitary oscillation probability. As we said above, the detector works between 100-10000 GeV, and the baseline is 480 m. it is easy to see that with this configuration we have

$$\frac{\Delta m^2 L}{E} << 1. \tag{5.2}$$

We use the equation above in Eq. (3.29) to get the zero-distance approximation shown in Eq. (3.30). Taking into account this approximation, the χ^2 is

$$\chi^2 = \sum_{\alpha=e}^{\tau} \frac{(N_\alpha^{\rm NU} - N_\alpha^{\rm exp})^2}{\sigma_\alpha^2} + \sum_{ij} \frac{(\alpha_{ij} - \delta_{ij})^2}{\sigma_{ij}^2}, \tag{5.3}$$

where, in the first summation, N_α^{exp} is the expected measured number of events per neutrino flavor, N_α^{NU} is the number of events computed in the presence of non-unitary, and the index α refers to the lepton flavor. The σ_α is the total uncertainty, statistical and systematical. Despite the uncertainties reported from the FASER collaboration, we symmetrize the uncertainties (In the case of $FASER\nu$ detector) and for the case of the FASERν2, we consider two scenarios, 5% and 10% as the systematical uncertainty, due to the expected improvement in the flux estimation by the time the experiment starts taking data.

To have a robust analysis, we are going to consider the three observables that FASERν will measure, for this reason, we need to consider all the appearance and disappearance channels. As a consequence, we have 6 non-unitary parameters that we must add to the analysis, and we have more free parameters than observables, so we need to consider a statical prior, as a penalization, to perform the analysis. In Eq. (5.3), we have added the prior (the second sum) to the values of α_{ij} non-unitary parameters that will be marginalized in our χ^2 analysis using as uncertainties, σ_{ij}, the constraints reported in Ref. [25]. We use the constraints at 90% confidence level (C.L.), making our results conservative.

The expected number of events adding the non-unitary effects are defined as:

$$N_{\alpha}^{\mathrm{NU}} = \frac{1}{\alpha_{11}^2(\alpha_{22}^2 + |\alpha_{21}|^2)}\big(N_{\alpha}^{\mathrm{SM}} P_{\alpha\alpha} + \sum_{\beta\neq\alpha} P_{\alpha\beta} N_{\beta}^{\mathrm{SM}}\big), \tag{5.4}$$

where N_{α}^{SM} is the Standard Model number of events for each flavor. $P_{\alpha\alpha}$ and $P_{\alpha\beta}$ are the disappearance and appearance probabilities in the approximation of the zero-distance, Eq. (3.19). The prefactor in Eq. (5.4) is the extra contribution of the NHLs to the effective μ constant, G_{μ}, that is mentioned in Chapter 2.

Since we consider all the non-unitary parameters at a time, the disappearance events may compensate for the appearance events, preventing them from having a visible effect. We will consider only one parameter at-a-time and marginalize the other 5 non-unitary parameters. It is important to recall that the α_{ij} parameters satisfy a triangle inequality condition, as described in Chapter. We incorporate these three inequalities into the computation of the χ^2.

5.4 Results

In this section, we will show the χ^2 analysis results and the sensitivity of the non-unitary parameters in FASERν and FASERν2 in two different energy regimes. We illustrate the expected FASERν sensitivity in Fig. 5.2. It is important to remember that the second scenario removes big uncertainties of the analysis and this could be reflected in a more restrictive sensitivity in the non-unitary parameters. We can observe that in FASERν the α_{33} parameter is not in the analysis because we do not have enough statistics in the ν_{τ} events. For the FASERν2, we still use the reduced energy regime (100-600 GeV), because we understand that the big uncertainties remain in the second phase of the experiment. In Fig. 5.3, we show the results of the FASERν2. The use of all the disappearance and appearance channels, with a prior that penalizes the α parameters (using as an uncertainty the current limits) gives us a realistic projection of the FASERν and FASERν2 sensitivity in the non-unitary parameters.

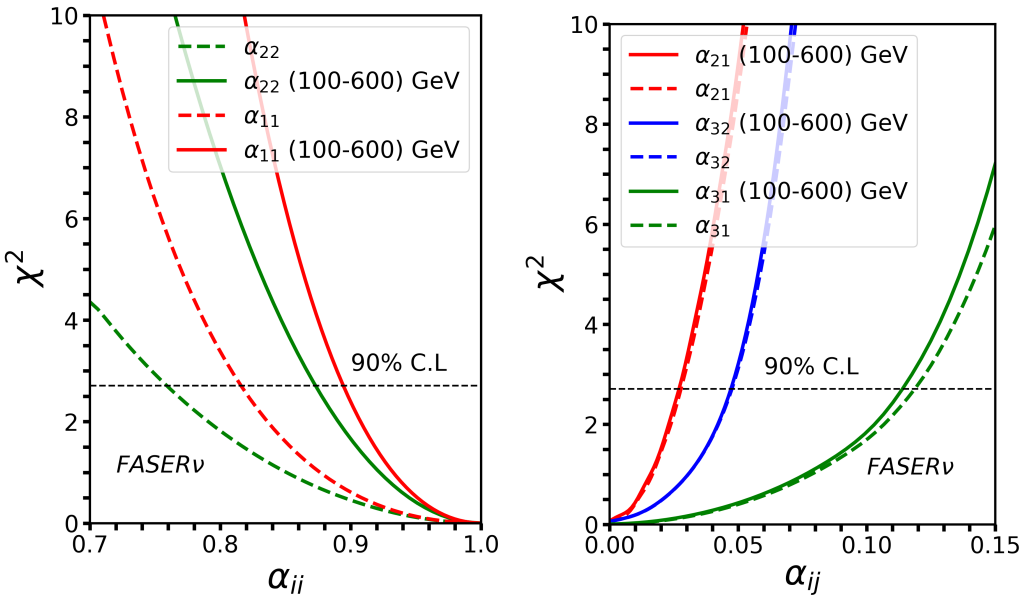

Figure 5.2: Sensitivity of the diagonal (left panel) and non-diagonal (right panel) non-unitarity parameters in the FASERν detector. The dashed curves and the solid curves show the sensitivity for the full FASERν energy window and the more restricted case with events between 100-600 GeV, respectively. The horizontal line represents the 90% C.L. for one free parameter according to [23].

Table 5.2 shows the expected sensitivity of the non-unitary parameters for all the cases at 90% C.L. We can observe that the FASERν future sensitivity does not improve the current limits. However, the limits in the 100-600 GeV regime have better sensitivity than using the full energy spectrum.

The FASERν 2 expects more restricted results than the FASERν detector and in fact, in the α_{11} and α_{33} parameters their sensitivity are better than the current constraint. Focusing on the disappearance of the ν_e and ν_τ channels will be crucial for placing constraints on these parameters. This could provide a valuable opportunity to shed light on the non-unitary parameters. We can see these results in Table 5.2 and Fig. 5.3.

The FASERν2 sensitivity can play a key role in constraining the non-unitary parameters and must be useful for a global analysis. The FASERν2 has the purpose of collecting a high statistic of neutrino events and, for that reason, it is plausible to reduce the systematical uncertainties to the levels we talk about in the work.

It is important to notice that this analysis was made to see the experiment's

	FASERν		FASERν2		
Parameter	$10^2 - 10^4$ GeV	100 – 600 GeV	100 – 600 GeV (5%)	100 – 600 GeV (10%)	Current limit
$\alpha_{11} \geq$	0.818	0.894	0.970	0.944	0.969
$\alpha_{22} \geq$	0.760	0.873	0.944	0.928	0.995
$\alpha_{33} \geq$	–	–	0.945	0.932	0.890
$\alpha_{21} \leq$	0.028	0.027	0.022	0.025	0.013
$\alpha_{31} \leq$	0.118	0.114	0.083	0.089	0.033
$\alpha_{32} \leq$	0.048	0.048	0.042	0.043	0.009

Table 5.2: Expected sensitivities for the α_{ij} non-unitary parameters for the case of FASERν and FASERν2 in different configurations [23]. The constraint on α_{33} is not shown for FASERν because there is no expected sensitivity. We also show for reference, in the last column, the current constraints reported in Ref. [25]. The results are shown at 90% C.L.

sensitivity to an indirect signature for NHL through the non-unitary parameters. In this work, we are not searching for direct signatures of these NHLs. We also recall, as noted in Chapter 2, that the standard oscillation probability for three flavors and three massive states is recovered when the diagonal α parameters approach one and the off-diagonal parameters approach zero. In this context, we consider a sensitivity to be more restrictive than other experiments when the constraints are closer to these SM limit values for a given confidence level.

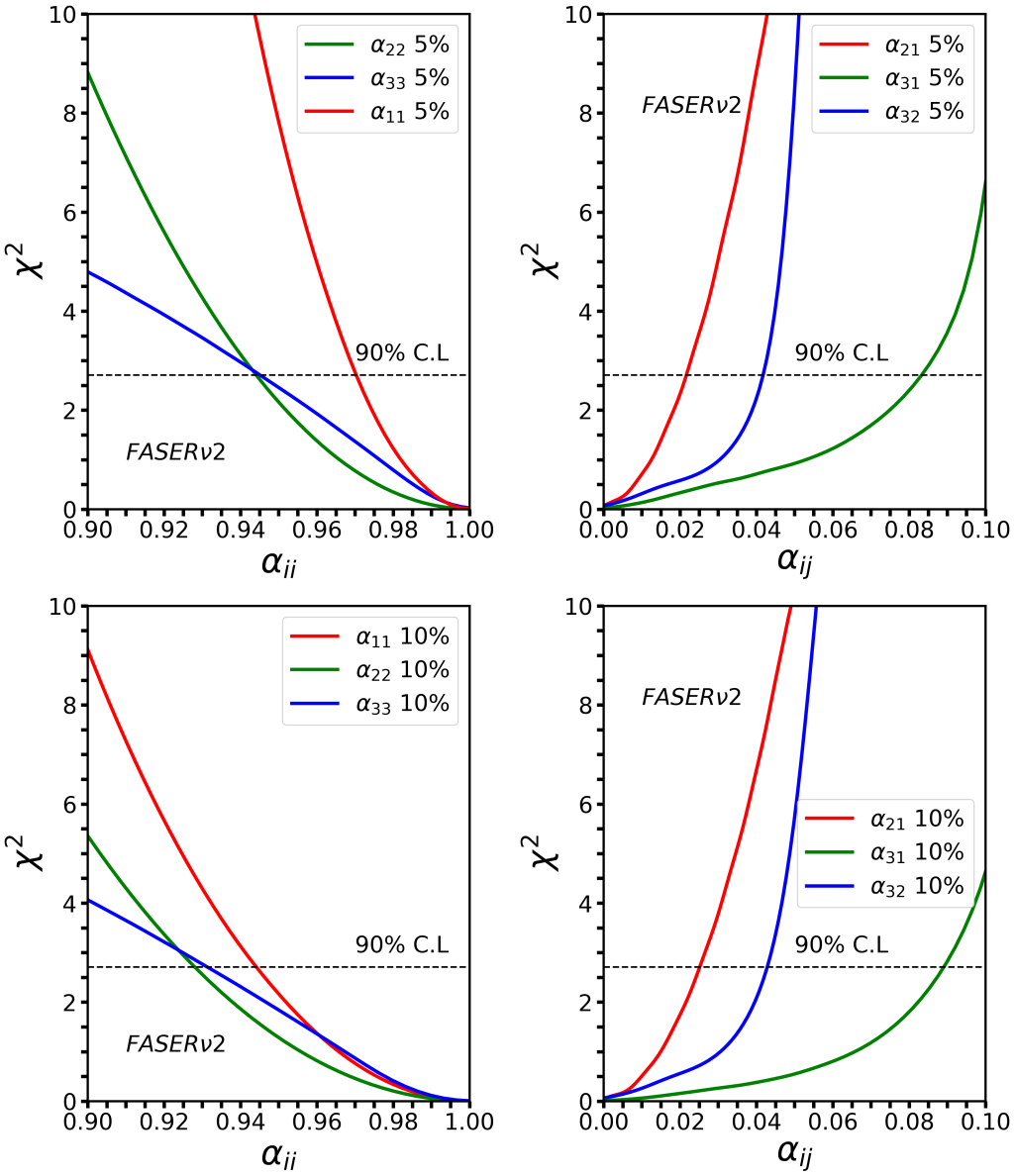

Figure 5.3: Left panel: sensitivity regions to the diagonal non-unitary parameters for the FASERν2 experiment. Right panels: the non-diagonal parameters case. For the upper panels we consider a systematic uncertainty of 5% while in the lower panels the 10% case is shown. The 90% C.L. is shown with a horizontal line [23].

Chapter 6

The Non-Unitary Effects in the Linear Seesaw Mechanism Constrained by the cLFV Processes

In the literature, various approaches have been proposed to constrain the non-unitary parameters in neutrino experiments [10–18]. However, as shown in Eq. (4.71), constraints can be translated from one parametrization to another. This opens up new possibilities for studying non-unitary parameters within specific models, such as the linear seesaw, by leveraging constraints from other observables, such as experimental limits on cLFV branching ratios, to further restrict the non-unitary parameters and then translate the constraint to the α parameters. These cLFV processes can be described as $\ell_i \longrightarrow \ell_j \gamma$, where the mediator is the NHL particle, as shown in Fig. 6.1. In this chapter, we will use the current and future experimental constraints of the cLFV branching ratios to obtain restrictions on the non-unitary parameters. We will show the explicit dependence of the branching ratios on the mixing neutrino matrix and relate them to the non-unitary effects in the light neutrino sector. For other works with a similar approach in the literature, see Refs. [14, 35–37, 48].

We will construct the neutrino mass matrix for the Linear seesaw mechanism. Afterward, we will use the Block Matrix Diagonalization Method (BMDM) approximation to diagonalize this matrix and obtain the mixing matrix and the physical neutrino masses. The next step will be computing the branching ratio of the cLFV processes and we will use the reported limits to obtain the current non-unitary constraints and the expected future sensitivity. Finally, we will translate these seesaw type I non-unitary constraints into model-independent parametrization results.

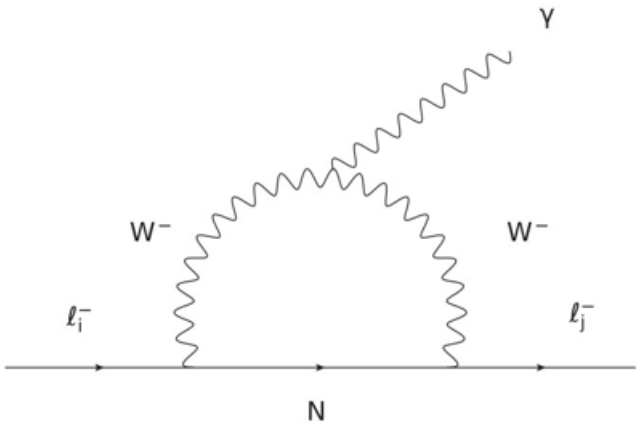

Figure 6.1: The cLFV processes, where ℓ_i could be τ, μ and ℓ_j could be μ, e.

6.1 Charged Lepton flavor Violation Processes (cLFV)

As we said above we will use the $\ell i \longrightarrow \ell_j \gamma$ processes, the branching ratio of these decays are [49–51]

$$BR(\ell \longrightarrow \ell'\gamma) = \frac{\alpha}{\gamma_\ell} m_\ell^3 |F_M^\gamma(0)|^2, \tag{6.1}$$

$$F_M^\gamma(0) = \frac{\alpha_W}{16\pi}\frac{m_\ell}{M_W^2}\sum_i K_{\ell i}^* K_{\ell' i} f_M^\gamma(x_i),$$

$$f_M^\gamma(x_i) = \frac{3x^3 log x}{2(x-1)^4} - \frac{2x^3+5x^2-x}{4(x-1)^3} + \frac{5}{6}.$$

Where $x_i \equiv m_{\chi_i}^2/M_W^2$ and m_{χ_i} are the physical masses of the neutrino states, $\alpha = e^2/4\pi$ is the fine-structure constant, and $\alpha_W \equiv \alpha/s_W^2$. Table 6.1 shows the current and future constraints of these processes, these limits will be used to constrain the non-unitary effects in the linear seesaw. It is important to notice that the sum in the previous branching ratio is over the number of neutrino massive states, for the case of the linear seesaw model it would be nine states. To compute the branching ratio we need to diagonalize the mass matrix of the linear seesaw, and for that reason, we make assumptions to obtain the mass matrix numerically.

6.2 Numerical Analysis

As we see in Chapter 3 the mass matrix of the linear seesaw depends on the M_L, M_D, and M. For each matrix, we have 18 free parameters that came from the 9 components, and each component could have a real and imaginary part. For this

Process	Present limit	Future Sensitivity
$\mu \longrightarrow e\gamma$	4.2×10^{-13} [52]	6×10^{-14} [53]
$\tau \longrightarrow e\gamma$	3.3×10^{-8} [54]	3×10^{-9} [55]
$\tau \longrightarrow \mu\gamma$	4.2×10^{-8} [54]	10^{-9} [55]

Table 6.1: The present and future sensitivity in the cLFV processes that will be used to constrain the non-unitary effects, this table was taken of [35]

reason, we need to assume some structure for the matrices, to remove some degrees of freedom due to our limited computational power. In this analysis, the matrices M_L and M are considered diagonals and their components are real as follows

$$M_{3\times3} = v_M \cdot diag(1+\epsilon_{M_{11}}, 1+\epsilon_{M_{22}}, 1+\epsilon_{M_{22}}), \tag{6.2}$$
$$M_L = v_L diag(1+\epsilon_{L_{11}}, 1+\epsilon_{L_{22}}, 1+\epsilon_{L_{33}}), \tag{6.3}$$

where v_{SM} is the SM vacuum expectation value (vev), and the v_M is the mass scale for the heavy sector. We decided to put the new physics in the structure of the M_D and use the Casas-Ibarra parametrization.

6.2.1 The Casas-Ibarra Parametrization

The idea behind this parametrization is to define the M_D matrix in terms of M_L and M, using the light mass equation of the linear seesaw model. However, this parametrization could be used in other models like the inverse seesaw[56]. For the case of the linear seesaw, we are going to use Eq. (4.27)

$$\begin{aligned} m_{\nu_{3\times3}} &= V_1^* m_{diag} V_1^\dagger = M_D(M_L M^{-1})^T + (M_L M^{-1}) M_D^T, \\ I =& (\sqrt{m_{diag}})^{-1} V_1^T M_D (M_L M^{-1})^T V_1 (\sqrt{m_{diag}})^{-1} \\ &+ (\sqrt{m_{diag}})^{-1} V_1^T (M_L M^{-1}) M_D^T V_1 (\sqrt{m_{diag}})^{-1}. \end{aligned} \tag{6.4}$$

We can rewrite the last equation as follows:

$$I = A + A^T, \tag{6.5}$$

where A takes the form

$$A = \begin{pmatrix} \frac{1}{2} & -a & -b \\ a & \frac{1}{2} & -c \\ b & c & \frac{1}{2} \end{pmatrix}, \tag{6.6}$$

where a, b, and c are real numbers. Now we can get the M_D matrix using the equation above, and we get

$$M_D = V_1^* \sqrt{m_\nu^{diag}} A^T \sqrt{m_\nu^{diag}} V_1^{*T} (M_L^T)^{-1} M^T. \tag{6.7}$$

For completeness, we can do the same for the inverse seesaw. In that case, we have

$$\begin{aligned} m_{\nu_{3\times3}} &= V_1^* m_{diag} V_1^\dagger = (M_D (M^T)^{-1} \mu M^{-1} M_D^T)_{3\times3}, \\ I &= \sqrt{m_{diag}})^{-1} V_1^T (M_D (M^T)^{-1} (\sqrt{\mu})^T \sqrt{\mu} M^{-1} M_D^T)_{3\times3} V_1 (\sqrt{m_{diag}})^{-1}, \\ I &= (\sqrt{\mu} M^{-1} M_D^T V_1 (\sqrt{m_{diag}})^{-1})^T (\sqrt{\mu} M^{-1} M_D^T V_1 (\sqrt{m_{diag}})^{-1}). \end{aligned} \tag{6.8}$$

We can rewrite the last equation as follows:

$$I = R^T R. \tag{6.9}$$

Where R is an orthogonal matrix, now we can express the M_D in terms of the other matrices

$$M_D = V_1^* \sqrt{m_{diag}} R^T (\sqrt{\mu})^{-1} M^T. \tag{6.10}$$

In this way, some works have studied the inverse seesaw phenomenology [35, 37].

6.3 Numerical Scan

We are using the BMDM approximation to obtain the light and heavy masses. In this case, for the light sector, we have a prescription for the diagonal mass matrix in terms of the light neutrino mixing matrix. In contrast, for the heavy sector, we must compute the diagonalization numerically. To compute the branching ratio we need to perform a random scan for the free parameters that we have in our model.

- To construct the light neutrino mixing we need three mixing angles, the CP phase, the Δm^2, and m_1 (the lightest massive state). We will use the oscillation data at 3σ to perform the random scan. We will also analyze the inverted hierarchy. We show the values of the mixing angles and the CP phase in Table 6.2.
- The $\epsilon_{M_{ii}}$ and $\epsilon_{L_{ii}}$ parameters are varied randomly from -0.5 to 0.5.
- The v_L scale is varied in the range of $[10^{-1} - 10^2]$ eV.
- The v_M is fixed at 1 TeV.
- The real parameters a, b, and c are varied in the range of $(0 - 10^{-2}]$ to respect the scale of the light masses.

Additionally, we put a condition for the M_D matrix to guarantee that the mass scales between the different matrices are fulfilled and that the Yukawas coupling is around one, as the naturalness argument tells us. Finally, we compute numerically the diagonalization of the heavy sector of the linear seesaw mass matrix. Then, we get the physical masses for the NHLs and compute the branching ratio of the cLFV processes using the Eqs. (4.8) and (6.1). Also, we can get the non-unitary effects using Eq. (4.15).

6.4 Results

In this section, we show the results of the analysis using the structure and scan described above. We first compute the branching ratio for the process $\mu \to e\gamma$ in terms of the v_L. We show this result in Fig. 6.2. We notice that the current and future limit of $Br(\mu \to e\gamma)$ restricts the v_L to be above 10 eV. We use the $\mu \longrightarrow e\gamma$ process because it has the most restricted limits. Using Eq. (4.15), we compute the off-diagonal non-unitary parameters for each process under both normal and inverted ordering. The results are presented in Figs. 6.3 and 6.4.

As mentioned above, the $Br(\mu \to e\gamma)$ process is more restrictive and, consequently, the non-unitary parameters will also be more constrained compared to the other two processes. Also, we see a correlation in some cases; for example, α_{21} in $\mu \longrightarrow e\gamma$, α_{31} in $\tau \longrightarrow e\gamma$, α_{32} in $\tau \longrightarrow \mu\gamma$. We notice the importance of off-diagonal non-unitary parameters in the cLFV processes. In the next chapter, we talk about how we can suppress the cLFV processes with non-unitary parameters.

In tables 6.3 and 6.4, we put the constraints of each off-diagonal parameter for each process and each ordering of the neutrino masses. We can conclude that, in the case of $\mu \longrightarrow e\gamma$, the non-unitary parameters are of the order of 10^{-5} and the other processes give us complementary results with bigger constraints for these parameters than the ones that come from neutrino experiments [25]. We can compare the restrictions between parametrizations using the Eq. (4.71). In Table 6.5, we see the constraints in the α parametrization. As in the case of the η parametrization, the $\mu \longrightarrow e\gamma$ gives us the most restricted results. These off-diagonal *alpha* parameters have better constraints than the current limits [25].

The cLFV processes could be a great observable to constrain the non-unitary parameters using the branching ratio of the processes. We see that the cLFV processes give us better constraints than the current ones that came from neutrino experiments. These results must encourage the search for these channels.

Parameters	Normal ordering at 3σ	Inverse ordering at 3σ
$\Delta m^2_{21}(eV^2)$	$(6.94 - 8.14) \times 10^{-5}$	$(6.94 - 8.14) \times 10^{-5}$
$\Delta m^2_{31}(eV^2)$	$(2.47 - 2.63) \times 10^{-3}$	$(2.37 - 2.53) \times 10^{-3}$
$\theta_{12}/^\circ$	31.4-37.4	31.4-37.4
$\theta_{23}/^\circ$	41.2-51.33	41.16-51.25
$\theta_{13}/^\circ$	8.13-8.92	8.17-8.96
$\delta/^\circ$	128-359	200-353

Table 6.2: Allowed parameter range, at 3σ [57] level, for the mixing angles, CP-violating phase, and neutrino mass differences. We use this range for the scan of light neutrino mixing in this scenario.

Parameters	$\mu \longrightarrow e\gamma$		$\tau \longrightarrow e\gamma$		$\tau \longrightarrow \mu\gamma$	
	Current	Future	Current	Future	Current	Future
$\lvert\eta_{12}\rvert \lessapprox$	2×10^{-5}	10^{-5}	2×10^{-2}	10^{-2}	2×10^{-2}	5×10^{-3}
$\lvert\eta_{13}\rvert \lessapprox$	2×10^{-4}	6×10^{-5}	10^{-2}	3×10^{-3}	2×10^{-2}	7×10^{-3}
$\lvert\eta_{23}\rvert \lessapprox$	4×10^{-4}	2×10^{-4}	3×10^{-2}	2×10^{-2}	10^{-2}	2×10^{-3}

Table 6.3: The current and future sensitivity for the off-diagonal parameters from the different cLFV processes in the normal ordering case.

Parameters	$\mu \longrightarrow e\gamma$		$\tau \longrightarrow e\gamma$		$\tau \longrightarrow \mu\gamma$	
	Current	Future	Current	Future	Current	Future
$\lvert\eta_{12}\rvert \lessapprox$	2×10^{-5}	10^{-5}	2×10^{-2}	10^{-2}	2×10^{-2}	10^{-2}
$\lvert\eta_{13}\rvert \lessapprox$	2×10^{-4}	6×10^{-5}	10^{-2}	3×10^{-3}	2×10^{-2}	7×10^{-3}
$\lvert\eta_{23}\rvert \lessapprox$	2×10^{-4}	7×10^{-5}	3×10^{-2}	2×10^{-2}	10^{-2}	2×10^{-3}

Table 6.4: The current and future sensitivity for the off-diagonal parameters from the different cLFV processes in the inverse ordering case.

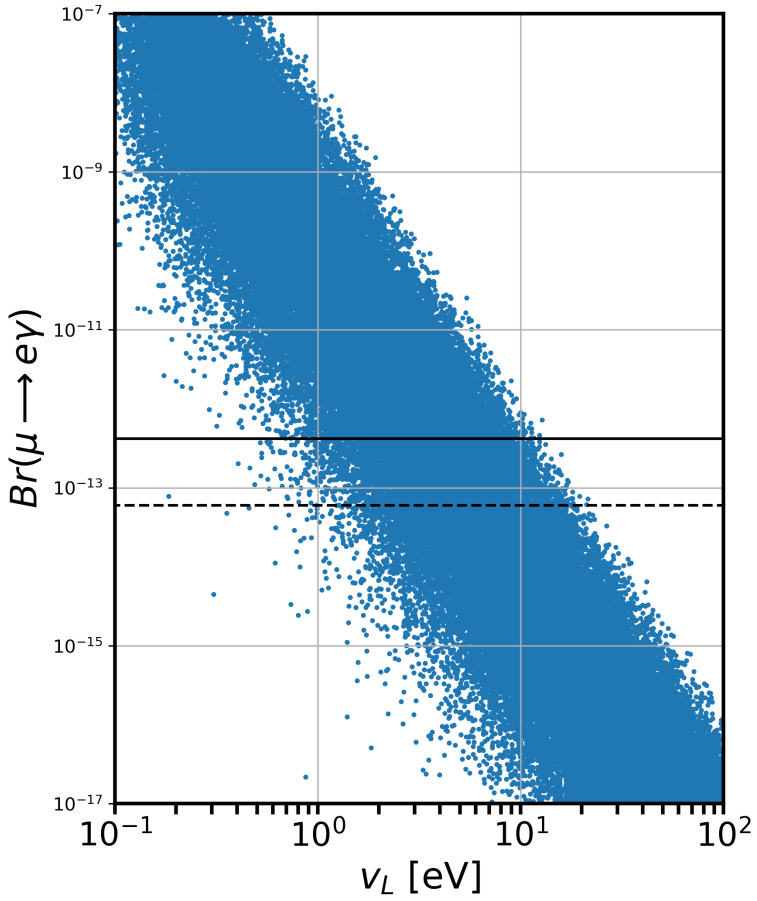

Figure 6.2: Branching ratio of the $\mu \to e\gamma$ decay vs the M_L scale in the normal ordering case. The solid line is for the current constraint, while the dashed one represents the future expected sensitivity for this decay.

Parameters	$\mu \longrightarrow e\gamma$		$\tau \longrightarrow e\gamma$		$\tau \longrightarrow \mu\gamma$	
	Current	Future	Current	Future	Current	Future
$\lvert\alpha_{12}\rvert \lessapprox$	4×10^{-5}	2×10^{-5}	4×10^{-2}	2×10^{-2}	4×10^{-2}	10^{-2}
$\lvert\alpha_{13}\rvert \lessapprox$	4×10^{-4}	1.2×10^{-4}	2×10^{-2}	6×10^{-3}	4×10^{-2}	1.4×10^{-2}
$\lvert\alpha_{23}\rvert \lessapprox$	8×10^{-4}	4×10^{-4}	6×10^{-2}	4×10^{-2}	2×10^{-2}	4×10^{-3}

Table 6.5: The current and the future sensitivity for the α off-diagonal parameters from the different cLFV processes in the normal ordering case.

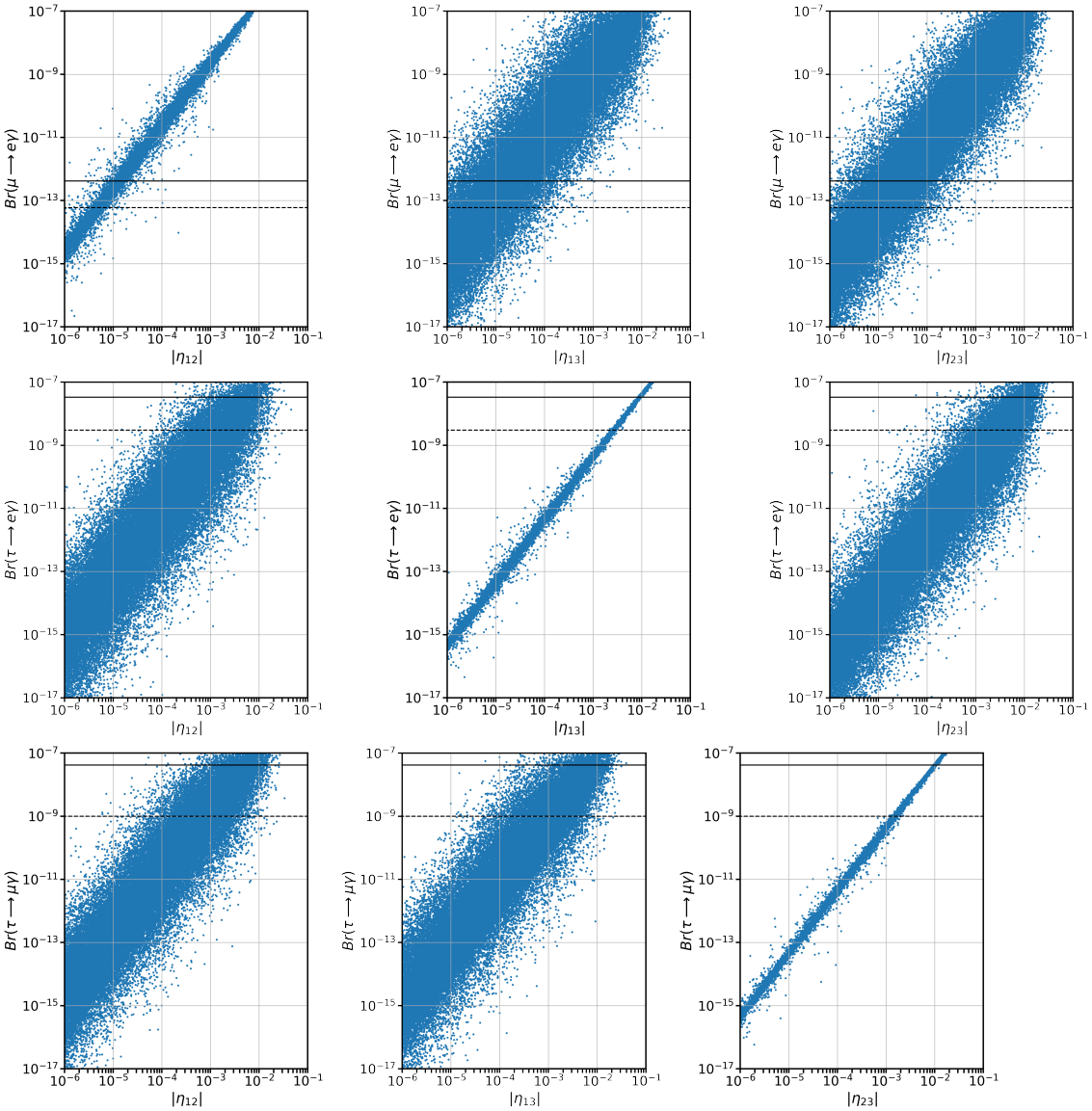

Figure 6.3: Scan of the branching ratio for the processes $\ell_i \longrightarrow \ell_j\gamma$ versus the nonunitary parameters in the normal ordering case. The solid is for the current constraints, while the dashed ones represent these decay's expected sensitivity according to [42].

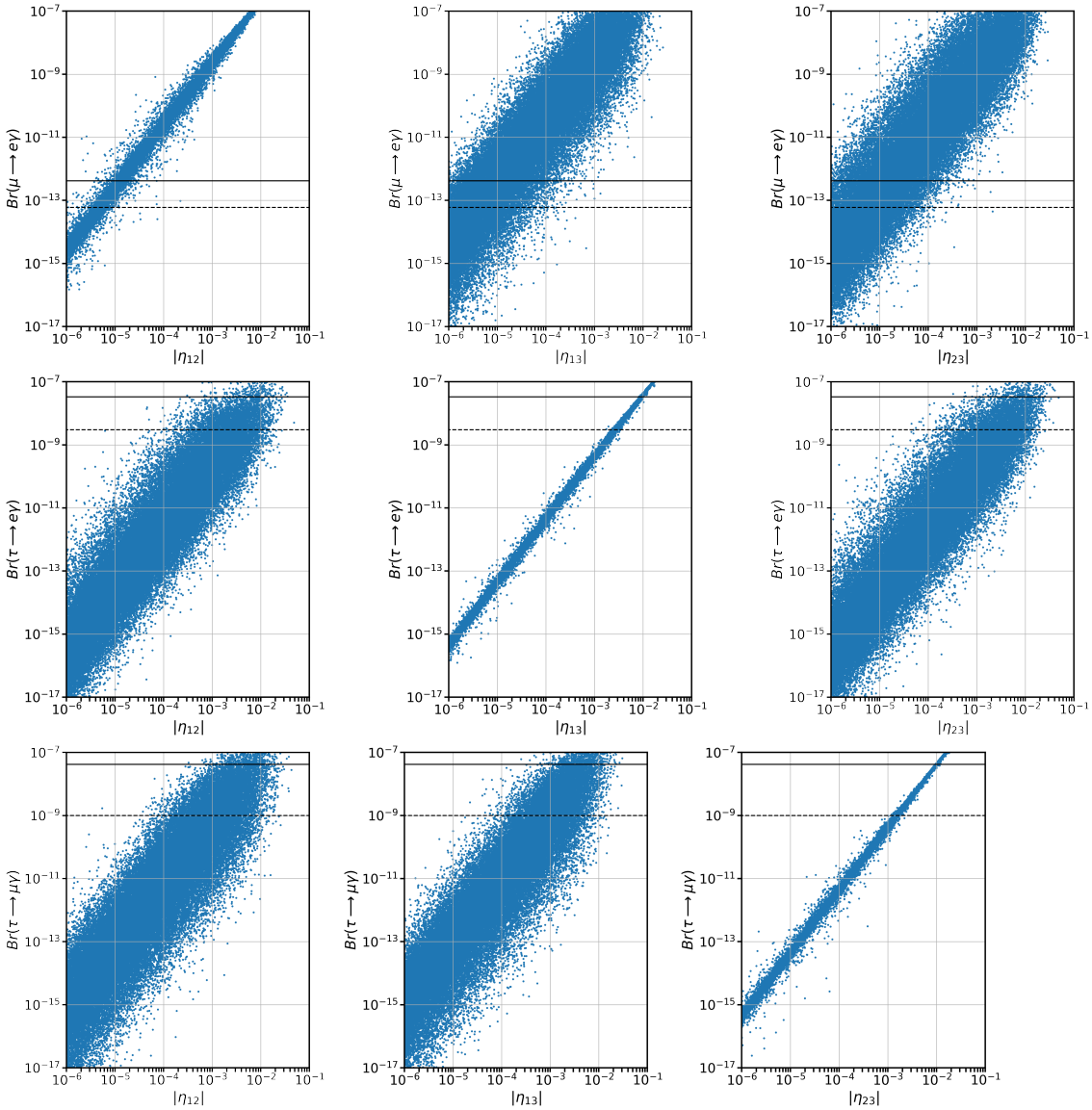

Figure 6.4: Scan of the branching ratio for the processes $\ell_i \longrightarrow \ell_j\gamma$ versus the nonunitary parameters in the inverse ordering case. The solid line accounts for the current constraints, while the dashed ones represent the future expected sensitivity for these decays [42].

Chapter 7

The cLFV Suppression Via Non-Unitary Effects

The cLFV processes are intrinsically related to the non-unitary effects. An example is the correlation that we can see in the last chapter between the processes and the non-unitary parameters in some cases. In [35], the authors explore a parametrization where the η matrix is diagonal (Eq. 4.15) and, as a consequence, the cLFV processes are suppressed. The easy way to produce this outcome is to assume that the M_D and M matrices are diagonal and all the new physics come from the μ and M_L for the inverse and linear seesaw, respectively.

However, in this work, we will diagonalize the full mass matrix for each model (Linear and Inverse seesaw) and we will study the suppression under the cLFV processes. We will compare the results using the full mass matrix diagonalization and the BMDM approximation to ensure that both methods agree and we will use the non-unitary parameter current limits to constrain the heavy scale of the model.

Moreover, we can control which channels are allowed by introducing off-diagonal parameters into the M matrix. Appendices A and B present models that explain the suppression of cLFV processes or enable only specific channels. The purpose of this analysis is to constrain the parameter space by combining branching ratio limits with non-unitary bounds derived from neutrino experiments.

7.1 The Mass Matrix Parametrization

According to [35], we can suppress the cLFV processes if the non-unitary matrix is diagonal, showing us that we can have non-unitary effects without the cLFV pro-

cesses. Using the non-unitary limits instead of the branching of the cLFV processes, we could restrict the parameter space of the minimal and low-scale seesaw.

7.1.1 The mass parametrization to suppress the cLFV processes

As we said above, to suppress the cLFV processes, we need the non-unitary matrix to be diagonal, one of the ways to get that is to parametrize the M and M_D matrices as follows:

$$M_{3\times3} = v_M \cdot diag(1+\epsilon_{M_{11}}, 1+\epsilon_{M_{22}}, 1+\epsilon_{M_{22}}), \tag{7.1}$$

$$M_{D_{3\times3}} = \frac{v_{SM}}{\sqrt{2}} \cdot diag(Y_{11}, Y_{22}, Y_{33}), \tag{7.2}$$

where v_M is the heavy scale, $v_{SM} = 249$ GeV is the SM scale, the $\epsilon_{M_{ii}}$ and Y_{ii} are random variables. With this, we can compute the non-unitary effects in the BMDM approximation. On the other hand, to diagonalize the full mixing matrix of the inverse and linear seesaw, we need to give structure to the μ and M_L matrices respectively. Using the full diagonalization method, we need to find how it looks the non-unitary effects in terms of the neutrino mixing matrix. We can compute the non-unitary condition of the 3×3 light neutrino submatrix,

$$(NN^\dagger)_{3\times3} = (I-\eta)(I-\eta)^\dagger \tag{7.3}$$

In the case of the seesaw type I realization, and using the definition of the η matrix in the DBDM approximation of Eq. (4.15), we see that the η matrix is equal to their conjugate transpose matrix. Therefore, we can rewrite the previous equation as

$$(NN^\dagger)_{3\times3} = I - 2\eta + O(\eta^2) \tag{7.4}$$

$$\eta \approx \frac{1}{2}(I - (NN^\dagger)_{3\times3}). \tag{7.5}$$

We neglected second-order terms in the η matrix to get the Eq. (7.5). So, we need the full neutrino mixing to extract the light sector of it, to do so we need the μ and M_L matrices

Inverse Seesaw

The main goal is the diagonalization of the full mass matrix. This matrix depends on the model that we are using, for the case of the inverse seesaw we will use the Eq. (4.16) as the mass matrix. We already have discussed the structure of the M_D and M matrix. Therefore, we need to discuss now the case of the μ matrix. To give it

a structure, we will use the Eq. (4.19) and will remember that we can put the flavor mass matrix in terms of the physical masses, using the unitary transformations, and obtain

$$\mu = M^T M_D^{-1} U^*_{PMNS} diag(m_1, m_2, m_3) U^\dagger_{PMNS} (M_D^{-1})^T M, \tag{7.6}$$

where the U_{PMNS} is the 3×3 neutrino mixing matrix for the light sector and m_i are the physical masses.

Linear Seesaw

In this case, we will use Eq. (4.23) as the mass matrix. Our goal is to provide structure to the M_L matrix. While we would like to follow the same approach as in the inverse seesaw case, it is not possible to explicitly solve for M_L from Eq. (4.27). Nonetheless, we can interpret the flavor mass matrix, as in the previous chapter, as $m_\nu = A + A^T$. In this way, we can distribute the value of m_ν matrix between the M_L components. With this in mind, we generate the following parametrization,

$$M_L = \begin{pmatrix} \frac{M_{11}}{2M_{D_{11}}} m_{\nu_{11}} & \frac{M_{22}}{M_{D_{22}}} m_{\nu_{12}} \cdot x_1 & \frac{M_{33}}{M_{D_{33}}} m_{\nu_{13}} \cdot x_2 \\ \frac{M_{11}}{M_{D_{11}}} m_{\nu_{12}} \cdot (1 - x_1) & \frac{M_{22}}{2M_{D_{22}}} m_{\nu_{22}} & \frac{M_{33}}{M_{D_{33}}} m_{\nu_{23}} \cdot x_3 \\ \frac{M_{11}}{M_{D_{11}}} m_{\nu_{13}} \cdot (1 - x_2) & \frac{M_{22}}{M_{D_{22}}} m_{\nu_{23}} \cdot (1 - x_3) & \frac{M_{33}}{2M_{D_{33}}} m_{\nu_{33}} \end{pmatrix}, \tag{7.7}$$

where x_1, x_2, and x_3 are random numbers that give a percentage of the value of the m_ν components. Again, in this framework, we consider M_D and M are diagonal and real matrices. This means that $M_D = M_D^T = M_D^*$ and we can rewrite the M_L in terms of the non-unitary matrix η in the DBDM approximation, Eq. (4.15), as follows

$$M_L = \begin{pmatrix} \frac{1}{\sqrt{2}} \sqrt{|\eta^{-1}|}_{11} m_{\nu_{11}} & \sqrt{2|\eta^{-1}|}_{22} m_{\nu_{12}} \cdot x_1 & \sqrt{2|\eta^{-1}|}_{33} m_{\nu_{13}} \cdot x_2 \\ \sqrt{2|\eta^{-1}|}_{11} m_{\nu_{12}} \cdot (1 - x_1) & \frac{1}{\sqrt{2}} \sqrt{|\eta^{-1}|}_{22} m_{\nu_{22}} & \sqrt{2|\eta^{-1}|}_{33} m_{\nu_{23}} \cdot x_3 \\ \sqrt{2|\eta^{-1}|}_{11} m_{\nu_{13}} \cdot (1 - x_2) & \sqrt{2|\eta^{-1}|}_{22} m_{\nu_{23}} \cdot (1 - x_3) & \frac{1}{\sqrt{2}} \sqrt{|\eta^{-1}|}_{33} m_{\nu_{33}} \end{pmatrix}, \tag{7.8}$$

As we can see, we have three additional variables compared with the inverse seesaw case. The idea behind constructing the full mass matrix is to have the full neutrino mixing matrix and not an approximation. Also, to ensure that the full method is well-behaved, we will compare its results with those of the BMDM approximation. Once we are convinced of our method, we switch on one cLFV channel.

7.1.2 The Mass Parametrization Allowing One cLFV Process

The suppression of the cLFV processes comes from the choice to put M_D and M diagonal, so the easiest way to allow these processes is to generate off-diagonal terms in these matrices. We only put off-diagonal terms in the M matrix for model-building purposes. An important remark of this analysis is that we use only the inverse seesaw due to its simplicity. For this reason, we continue using Eqs. (7.1), (7.2), and (7.6) to construct the full mass matrix. As we saw in the last chapter, the cLFV processes are correlated with the off-diagonal non-unitary parameters. The $\mu \longrightarrow e\gamma$ process is related with η_{12}, the $\tau \longrightarrow e\gamma$ process is related with η_{13}, and the $\tau \longrightarrow \mu\gamma$ process is related with η_{23}. We will allow only one of these channels in each case, with the fewest parameters that our numerical analysis allows. This can be achieved using the following M matrices

$$M = v_M \begin{pmatrix} 1+\epsilon_{11} & 0 & 0 \\ 1+\epsilon_{21} & 1+\epsilon_{22} & 0 \\ 0 & 0 & 1+\epsilon_{33} \end{pmatrix}, \tag{7.9}$$

$$M = v_M \begin{pmatrix} 1+\epsilon_{11} & 0 & 0 \\ 0 & 1+\epsilon_{22} & 0 \\ 1+\epsilon_{31} & 0 & 1+\epsilon_{33} \end{pmatrix}, \tag{7.10}$$

$$M = v_M \begin{pmatrix} 1+\epsilon_{11} & 0 & 0 \\ 0 & 1+\epsilon_{22} & 0 \\ 0 & 1+\epsilon_{32} & 1+\epsilon_{33} \end{pmatrix}. \tag{7.11}$$

These M matrices allow the $\mu - e$, $\tau - e$, and $\tau - \mu$ processes, respectively. We notice that we only need one parameter in the analysis to allow these processes. Computationally, this does not represent any difficulty.

7.2 Numerical Scan of the free parameters

Up to now, we know the structure of the mass matrix, but not the running of the variables. In this section, we will discuss the parameter space of the variables that we use in the analysis.

7.2.1 parameter scan in the cLFV suppression case

Our numerical analysis for this chapter will be similar to one introduced in the previous chapter, but instead of having the M_L matrix diagonal, we will have the M_D matrix as a diagonal one. All the new physics information will be contained in the μ and M_L matrices for the inverse and linear seesaw, respectively. These matrices depend on the m_ν, M, and M_D matrices. All the variables that compound these matrices are random variables. We can notice that m_ν depends on the PMNS matrix and the neutrino physical masses, as we can see in Eq. (4.3). The PMNS matrix is generated using random values for the oscillation data, varying them up to 3σ. We can see this region for the PMNS values in Table 6.2. Here we enlist all the variables that we use in this analysis

- For the lightest mass state, we use the cosmological constraints that came from Table 6.2.
- The $\epsilon_{M_{ii}}$ and $\epsilon_{D_{ii}}$ parameters are varied randomly from -0.5 to 0.5 .
- The v_M scale is varied in the range of $[10^{10} - 10^{14}]$ eV.
- The v_{SM} is fixed at the SM scale ($\approx$ 249 Gev).
- The real parameters x_1,x_2, and x_3 are varied in the range of $[0 - 1]$, this parameters are used only in the linear model.

It is important to remember that each case has a different number of random variables. For example, to compute the non-unitary effects in the BMDM approximation we only need the M_D and M matrices, while for the full diagonalization, we need more parameters. The full mass diagonalization is performed using the Takagi decomposition to guarantee the non-negative real eigenvalues for a symmetric complex matrix using a Python routine with arbitrary accuracy. After the diagonalization of the mass matrix for each case, we need to use Eq. (7.5) to extract the non-unitary effects of the light neutrino sector.

7.2.2 Parameter Scan Allowing one cLFV channel

The numerical analysis with one cLFV process will be done using the inverse seesaw model due to its simplicity and the fact that the model has fewer parameters than the linear seesaw model. We will keep using the same parameters as in the inverse model above and only add one new parameter depending on which cLFV process we want to allow. These parameters will be in the off-diagonal components of the M matrix, as we can see in the Eqs. (7.9-7.11). Each new parameter is varied from -0.5 to 0.5. The cLFV processes open the possibility of constraining the parameter space due to the new non-unitary restrictions that we can use in this analysis.

7.3 Results

We are analyzing two scenarios. The first scenario assumes a diagonal non-unitary matrix, which suppresses all cLFV processes. For this analysis, we constructed a parametrization for the μ and M_L matrices to diagonalize the full mass matrix for the low-scale seesaw models and compare it with the BMDM approximation. In the second scenario, we allow only one cLFV process by introducing an off-diagonal component in the M matrix. In the first case, the primary objective of this analysis is to calculate the neutrino mixing matrix and constrain the heavy scale of the seesaw model using the non-unitary limits. The first scenario served as a test to validate the reliability of our numerical approach.

Consequently, for the second scenario, we focus solely on the inverse seesaw mechanism due to its straightforward implementation. The aim is to compute the branching ratio for each process using Eq. (6.1) and to constrain the parameter space in the inverse seesaw model by applying the experimental limits on the branching ratios and the non-unitary bounds coming from neutrino experiments. At the theory level, these phenomenological scenarios are explained in the Appendix A and B.

7.3.1 Suppressing all the cLFV processes

For this case, we compute the non-unitary effects using the BMDM and the full mass matrix diagonalization for the inverse and the linear seesaw cases. As we said, all the cLFV processes are forbidden. Therefore, we can not take advantage of the branching ratio constraints to restrict the parameter space. However, we can use the non-unitary constraints on $|\alpha_{22}|$ that comes from neutrino oscillation experiments [25] to restrict the parameter space and, more specifically, the scale of the heavy sector, as we can see in Fig. 7.1, that indicates that the heavy scale must be greater than 2 TeV. We only use this α_{22} constraint because it is the non-unitary parameter with the most restrictive limit and the other parameters do not have enough sensitivity.

We are confident that our method for the full-diagonalization matrix behaves correctly because we made the same analysis with the BMDM approximation and confirmed that each point in the parameter space coincides in both cases.

7.3.2 Allowing one cLFV process

As we said above, this analysis only uses the inverse seesaw model due to its simplicity. Now we can use the branching ratio and the non-unitary limits to constrain the parameter space of the three processes. In Fig. 7.2, we can see the parameter space of the processes in different planes. As we expected, the $\mu \to e\gamma$ process is

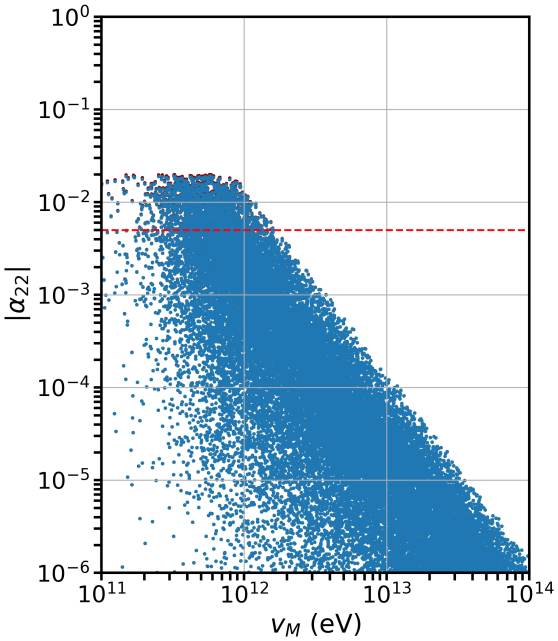

Figure 7.1: the vev vs the α_{22} using the BMDM and full diagonalization method of the inverse and linear models. The red line is the current limit of the α_{22} coming from the oscillation experiments [25]

very constrained by its limits. In the plane α_{22}-v_M (Fig. (7.3)) there are some points that, while being allowed by the branching ratio limits, are not when we consider the neutrino experiment constraints on α_{22}. These points are represented as red points in the plots.

On the other hand, we observe that the branching ratio limits can provide stricter constraints than those coming from neutrino experiments. Additionally, the branching ratio limits the α_{21} to values below 10^{-5} (see for instance the $|\alpha_{21}| - v_M$ plane). In the $Br(\mu \to e\gamma)$-$|\alpha_{22}|$ plane, we notice many points in the parameter space that are excluded by the current α_{22} limit. It is important to emphasize that, although not immediately apparent in this process, the branching ratio and non-unitary limits complement each other in constraining the parameter space.

In the case of $\tau \to e\gamma$, it is important to note that the parameter space excluded by the neutrino experiment constraint on α_{22} is larger than in the previous case. This is easy to see in the α_{22}-v_M and $Br(\tau \longrightarrow e\gamma)$-$\alpha_{22}$ planes. However, if we see the $Br(\tau \longrightarrow e\gamma)$-$|\alpha_{31}|$ planes it seems like the α_{22} constraints a big part of the parameter space of the process, this happens because the overlap effect in the plot. Additionally, the $Br(\tau \to e\gamma)$-$|\alpha_{31}|$ and α_{22}-v_M planes show that the limit on α_{31} coming from neutrino experiments restricts the same parameter space as the current limit on the branching ratio in the $\tau \to e\gamma$ process.

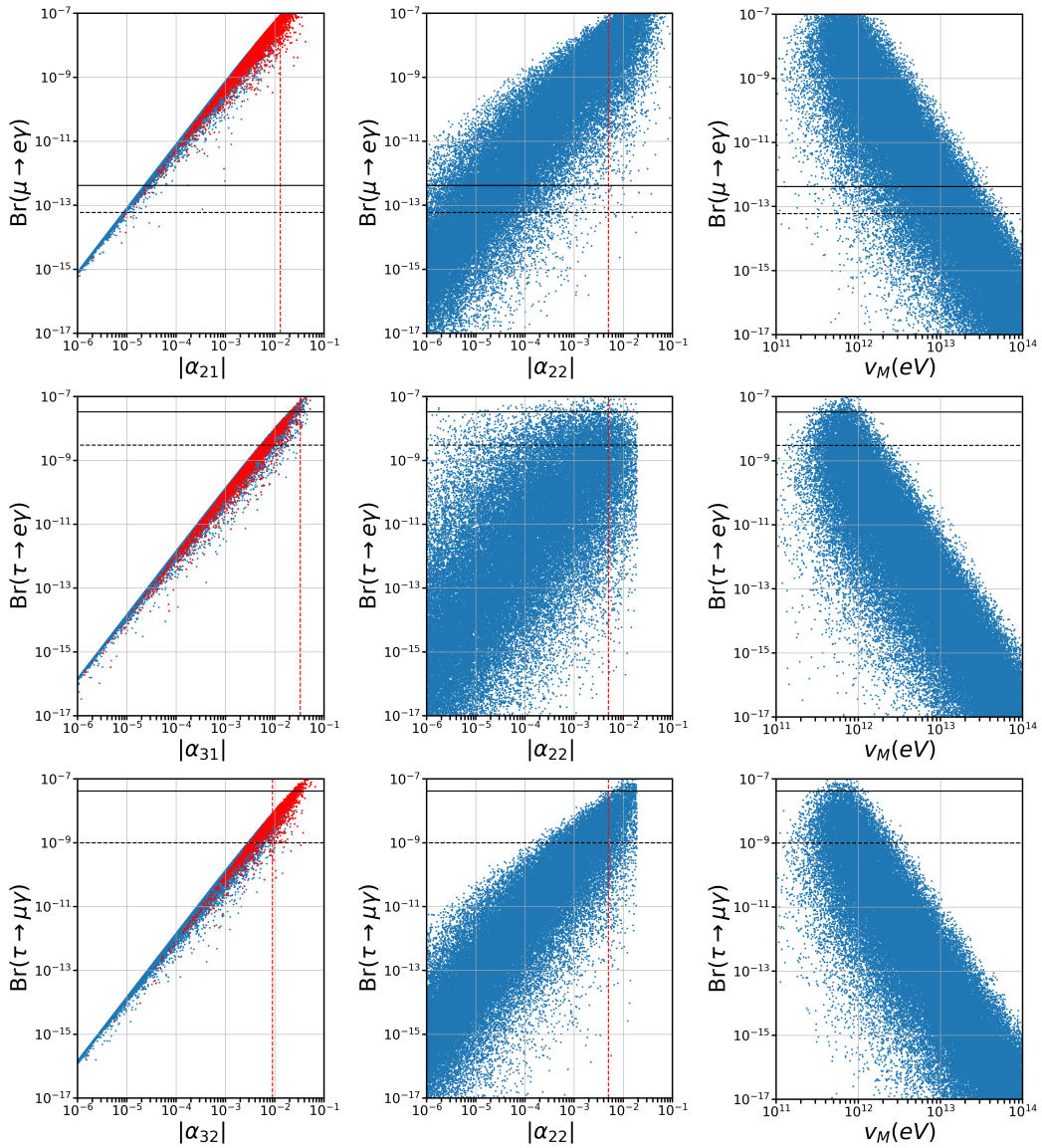

Figure 7.2: The parameter space of the $Br(\ell_i \longrightarrow \ell_j\gamma)$ using the current (black solid line) and future (black dashed line) constraints of each process and the non-unitary constraints that came from neutrino oscillation experiments. The red dashed lines are the current non-unitary parameter limit. Also, the red points are the ones forbidden by the α_{22} restriction.

The $Br(\tau \longrightarrow \mu\gamma)$ process gives us similar results as the $Br(\tau \longrightarrow e\gamma)$. We notice a big parameter space that is allowed by the branching limits, but it is not by the non-unitary limits. Also, we see the same overlap effect in the $Br(\tau \longrightarrow \mu\gamma)$-$|\alpha_{32}|$ plane. In this case, the α_{22} is not the only non-unitary parameter that constrains

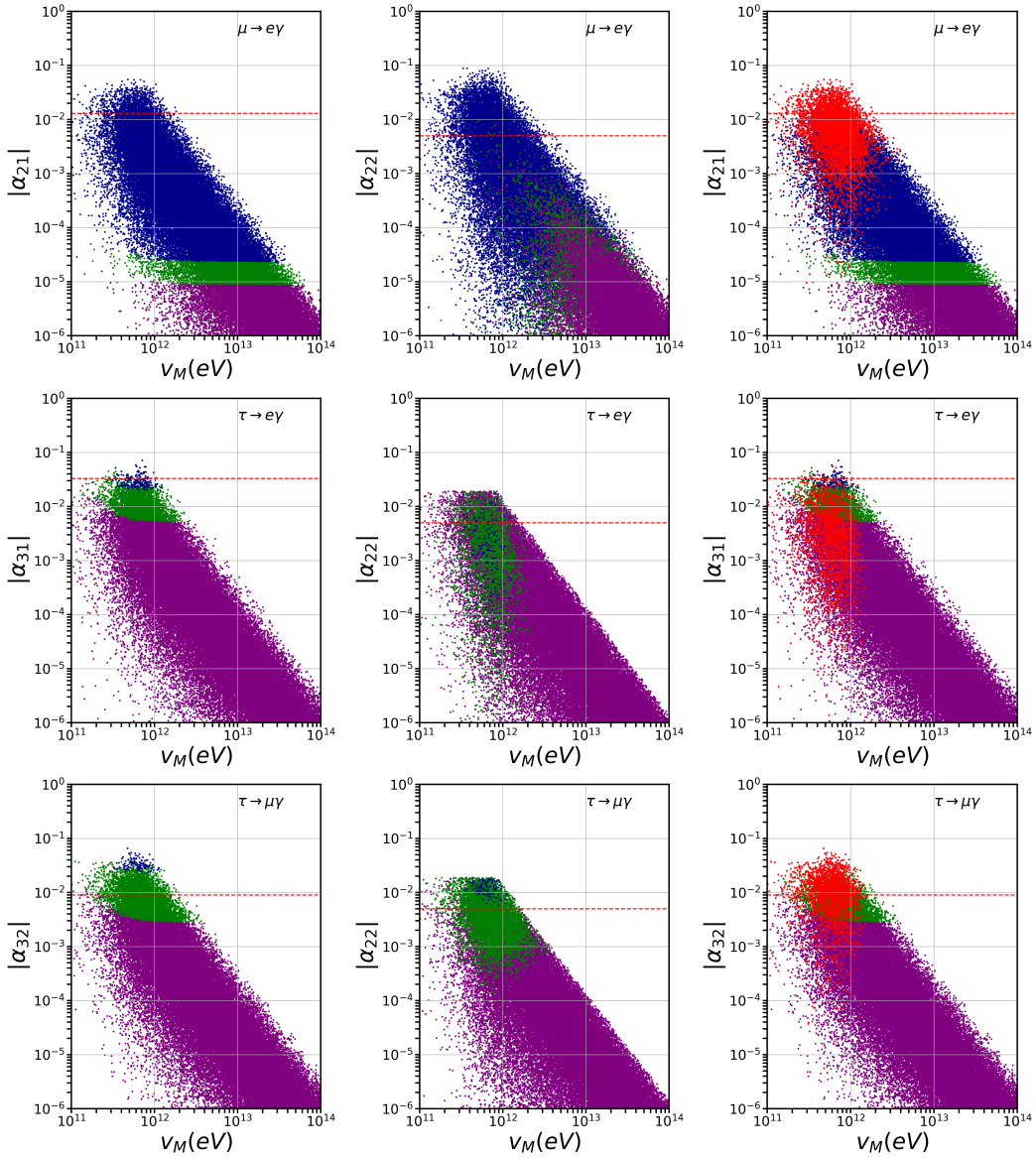

Figure 7.3: The parameter space of the $Br(\ell_i \longrightarrow \ell_j\gamma)$ in the $|\alpha_{ij}| - v_M$ planes. The red dashed lines are the current non-unitary limits, and the solid and dashed black lines are the future and current constraints of the processes. Also, the red points are the ones forbidden by the α_{22} restriction. The dark blue points show the parameter space forbidden by the current cLFV limits, the green points shows the additional exclusion by including future limits. The purple points are allowed by the future cLFV constraints [58].

phase space regions. If we see the α_{32}-v_M plane, we notice that α_{32} constrains more than the current branching limit and also, could restrict the parameter space. On

the right side of Fig 7.3 we see in the α_{32}-v_M plane that the α_{22} rules out almost the same region than the α_{32} parameters.

Additionally, it is important to note that the region excluded by α_{22} (that comes from neutrino experiments) tends to disfavor values for the heavy sterile neutrinos below 1 TeV across all channels [58].

Chapter 8

Conclusions

Non-unitary effects in the active sector of neutrino mixing arise when additional heavy neutral leptons are introduced into the theory. These effects depend on parameters associated with the new particles, which can be constrained through neutrino experiments. By analyzing both the appearance and disappearance channels for each neutrino flavor, we can identify possible anomalies in the neutrino event number that would be a signature of the presence of these non-unitary effects.

In this thesis, we have explored non-unitary sensitivities in various current and future experiments, as well as within different models. We analyzed the FASERν and FASERν2, where we explored the non-unitary effects using a model-independent (α) parametrization. We computed the neutrino number of events in the SM using the neutrino fluxes from [47], and with these values, we computed how the neutrino events changed with the new, zero-distance, oscillation probability for every channel (appearance and disappearance). To obtain a forecast of the FASERν sensitivity to non-unitary parameters, we compared the expected neutrino number of events in the SM case with those expected in the non-unitary framework, using a χ^2 analysis to quantify such a sensitivity. For FASERν, we analyzed two different scenarios, with the most restrictive one being the one with a reduced energy region. However, the resulting constraints are not competitive with the current limits. On the other hand, we performed a forecast for the FASERν2 experimental setup, considering both 5% and 10% systematic uncertainties. The results of $FASER\nu2$ are more encouraging, and in this case, we noticed that the α_{11} and α_{33} sensitivities are better than the current limits. We hope these results will help to encourage the FASER collaboration to improve their systematic uncertainties and pay attention to the e and τ disappearance channels.

There are other processes where the non-unitary effects are present, as we said

above, the non-unitary effects appear when we have additional massive states, as in the case of the seesaw type I mechanism. Besides the FASER case, we used the (current and future) limits of the Branching ratio of cLFV processes in the linear seesaw model to restrict the non-unitary effects in the η parametrization. We also translated these limits into the model-independent α parametrization and we saw that these results are two orders of magnitude more restrictive than the current limits in neutrino experiments.

Using alternative parametrizations for the mass matrices in the inverse seesaw mechanism [35], we can suppress the cLFV processes. Similarly, we developed a parametrization to observe the same phenomenology in the linear seesaw case. We used the current non-unitary limits for these scenarios to constrain the parameter space. However, the branching ratios and the non-unitary limits come from independent experiments and we can use them to restrict the parameter space of the low-scale seesaw models. Then, we described how we can switch on each cLFV process. Using the current limits we concluded that our analysis disfavor scales below the 1 TeV.

Non-unitary effects are fascinating observables, as they manifest in various models, such as the seesaw mechanism, and provide a means to constrain the parameter space. Remarkably, these effects can be studied even in experiments not specifically designed for neutrino oscillation, such as the FASERν detector. This highlights the significance of non-unitary effects as a valuable probe in particle physics, and we hope this work inspires further research in this area.

Appendix A

Models to Suppress the cLFV Processes

A.1 Linear Seesaw

In the linear seesaw mechanism, we consider three right-handed neutrinos, with B-L charge -1, and three left-handed sterile neutrinos with no lepton number. The Lagrangian of the linear seesaw is:

$$\mathcal{L}_{Yuk} = y_i^{(\ell)}\,\overline{\hat{L}_i}\,H\,\hat{\ell}_{Ri} + y_i^{(\nu)}\,\overline{\hat{L}_i}\,\tilde{H}\,\hat{N}_{Ri} + \tilde{y}_i^{(\nu)}\,\overline{\hat{L}_i}\,\tilde{H}\,\hat{S}_i^c + M_i^{(N)}\,\overline{\hat{S}_i}\,\hat{N}_{Ri} + h.c. \tag{A.1}$$

where,

$$H = \begin{pmatrix} H^+ \\ H^0 \end{pmatrix}, \quad H' = \begin{pmatrix} H'^+ \\ H'^0 \end{pmatrix}, \quad L_i = \begin{pmatrix} \nu_{Li} \\ \ell_i \end{pmatrix} \tag{A.2}$$

$\tilde{H} = i\sigma_2 H^*$ and $\tilde{H}' = i\sigma_2 H'^*$. We can notice that the $B-L$ symmetry forbids the Majorana mass term of the right-handed neutrinos. To forbid the Majorana mass of the left-handed sterile and to construct the M_D and M_R diagonals, we need to include a discrete group Z_n. All the fermions must transform non-trivially under the discrete group; for each lepton f we have: $f_1 \sim \omega^1$, $f_2 \sim \omega^2$, $f_3 \sim \omega^3$ where $f = L, N, S$ and the $\omega^N = 1$. To forbid any Majorana mass term, we need to fulfill the next condition $N > 6$ [58]. With this condition, we propose the model in the Table A.1.
The m_ν will have the next form:

$$m_\nu = \begin{pmatrix} 0 & 0 & \tilde{y}_1 v_2^3 \\ 0 & \tilde{y}_2 v_2^3 & \tilde{y}_4 v_2^2 \\ \tilde{y}_3 v_2^3 & \tilde{y}_5 v_2^2 & \tilde{y}_6 v_2^1 \end{pmatrix}. \tag{A.3}$$

this is the A_1 two-zero texture accordingly with [59]. This is compatible with

	L_e	L_μ	L_τ	l_e	l_μ	l_τ	N_1	N_2	N_3	S_1	S_2	S_3	H	H_2^i	ϕ
$SU(2)_L$	2	2	2	1	1	1	1	1	1	1	1	1	2	2	1
$U(1)_{B-L}$	-1	-1	-1	-1	-1	-1	-1	-1	-1	0	0	0	0	1	1
Z_7	ω	ω^2	ω^3	ω	ω^2	ω^3	ω	ω^2	ω^3	ω	ω^2	ω^3	1	ω, ω^2, ω^3	1

Table A.1: Linear seesaw model with three extra Higgs and one extra scalar field in accordance with [42].

the neutrino phenomenology as the neutrino oscillation and the restriction on the effective mass of the neutrinoless double beta decay [60–62]. To get the M_L mass term, we need to add more Higgs doublets, which needs B-L, and Z_7 charges to compensate the charges of S and N leptons. This is one way to get the M_D and M diagonals but it is not unique. It is important to remark that we work with a $U(1)_{B-L}$ symmetry that could be local, as a consequence new boson would be in the model.

A.2 Inverse Seesaw

The inverse seesaw model is well studied in [35]. However, we will summarize it and then extend this model to the case where we allow only one cLFV channel. As in the linear seesaw case, we will use the $B-L$ symmetry to forbid the Majorana term in the right-handed neutrino. This model has three right-handed neutrinos $\hat{N}_R$ with $B-L$ charge -1 and three sterile fermions $\hat{S}$. In this model, Lagrangian is:

$$\mathcal{L}_{Yuk} = y^{(\ell)}\,\overline{\hat{L}}\,H\,\hat{\ell}_R + y^{(\nu)}\,\overline{\hat{L}}\,\tilde{H}\,\hat{N}_R + M^{(N)}\,\overline{\hat{S}}\,\hat{N}_R + \mu\overline{\hat{S}}\hat{S}^c + h.c. \tag{A.4}$$

we can build a model that is allowed by the oscillation data and has a A_1 two-zero texture as in Eq. A.3 using the $U(1)_{B-L}\times Z_5$ symmetry. We use two scalar fields ξ and ϕ to break these symmetries. The μ matrix has the next form:

$$\mu = \begin{pmatrix} 0 & 0 & \tilde{y}_1 v_2^3 \\ 0 & \tilde{y}_2 v_2^3 & \mu_1 \\ \tilde{y}_1 v_2^3 & \mu_1 & \tilde{y}_3 v_2^1 \end{pmatrix}. \tag{A.5}$$

Where μ_1 are the Majorana mass terms that appear in the model. The ξ field generates the other components of this matrix. As in the linear seesaw case, the $U(1)_{B-L}$ can be local, so a Z' would be in the model.

	L_e	L_μ	L_τ	l_e	l_μ	l_τ	N_1	N_2	N_3	S_1	S_2	S_3	H	ξ	ϕ
$SU(2)_L$	2	2	2	1	1	1	1	1	1	1	1	1	2	1	1
$U(1)_{B-L}$	-1	-1	-1	-1	-1	-1	-1	-1	-1	0	0	0	0	0	1
Z_5	ω	ω^2	ω^3	ω	ω^2	ω^3	ω	ω^2	ω^3	ω	ω^2	ω^3	1	ω	1

Table A.2: Inverse-seesaw model with two scalar fields that broke the $U(1)_{B-L} \times Z_5$, in accordance with [35].

Appendix B

Models to Allow One cLFV Process

B.1 Linear Seesaw

If we want only one decay channel we need to add more particles to the model. The condition to allow the $\tau \longrightarrow e\gamma$ process using the same symmetries and charges that in the Table A.1 is to add a Higgs with charge ω^{-2} and change the charges of H_i' that are ω, ω^2, ω^5 and for this case, we have the same charge on the fermions.For this case the m_ν matrix structure is a B3 two-zero texture:

$$M_L = \begin{pmatrix} \tilde{y}_1 v_2^3 & 0 & \tilde{y}_2 v_2^3 \\ 0 & 0 & \tilde{y}_4 v_2^2 \\ \tilde{y}_3 v_2^3 & \tilde{y}_5 v_2^2 & \tilde{y}_6 v_2^1 \end{pmatrix}. \tag{B.1}$$

The two other processes have the same number of particles and the same charges in H_i' and the extra Higgs with charge ω^{-2}, but instead we need to permutate the Z_7 in the fermion sector. For the $\mu \longrightarrow e\gamma$ the Z_7 charges of the fermions are: $f_1 \sim \omega^1$, $f_2 \sim \omega^3$, $f_3 \sim \omega^2$ a consequence of this, the structure of the light neutrino mass matrix change to:

$$\nu_\mu = \begin{pmatrix} \tilde{y}_1 v_2^1 & \tilde{y}_1 v_2^2 & 0 \\ \tilde{y}_3 v_2^2 & \tilde{y}_2 v_2^3 & \tilde{y}_4 v_2^2 \\ 0 & \tilde{y}_5 v_2^2 & 0 \end{pmatrix}. \tag{B.2}$$

This is the so-called B_4 two-zero texture. At last, to allow the $\tau \longrightarrow \mu\gamma$ process and suppress the other two processes, we need to permutate again the Z_7 charges of the fermions as follows: $f_1 \sim \omega^3$, $f_2 \sim \omega^1$, $f_3 \sim \omega^2$, in this case the m_ν matrix has the A_1 two-zero texture (Eq. (A.3)), as in the model with all cLFV processes suppressed.

B.2 Inverse Seesaw

to allow only one channel we are going to use the same permutation of charges as in the linear seesaw due to the Lagrangian term that generates the M matrix being the same in both models. The field that generates the new terms that allow the processes for each case is a new scalar field with a charge ω^2. It is important to remark that this new extra scalar field would have a $B - L$ charge equal to zero, and for this reason, we can put a charge ω^2. In the case of $\tau \to e\gamma$ the m_ν matrix has the A_1 two-zero texture, the $\tau \to \mu\gamma$ has the B_3 two-zero texture and at last the $\mu \to e\gamma$ has a A_2 two zero texture in the m_ν that is described by the next equation:

$$\nu_\mu = \begin{pmatrix} 0 & \tilde{y}_1 v_2^3 & 0 \\ \tilde{y}_3 v_2^3 & \tilde{y}_2 v_2^3 & \tilde{y}_4 v_2^2 \\ 0 & \tilde{y}_5 v_2^2 & \tilde{y}_6 v_2^1 \end{pmatrix}. \tag{B.3}$$

Bibliography

1. Pal, P. B. *An Introductory Course of Particle Physics* ISBN: 978-0-429-06851-5 (CRC Press, July 2014).
2. Glashow, S. L. Partial Symmetries of Weak Interactions. *Nucl. Phys.* **22,** 579–588 (1961).
3. Weinberg, S. A Model of Leptons. *Phys. Rev. Lett.* **19,** 1264–1266 (1967).
4. Salam, A. Weak and Electromagnetic Interactions. *Conf. Proc. C* **680519,** 367–377 (1968).
5. Chatrchyan, S. *et al.* Observation of a New Boson at a Mass of 125 GeV with the CMS Experiment at the LHC. *Phys. Lett. B* **716,** 30–61. arXiv: 1207.7235 [hep-ex] (2012).
6. Aad, G. *et al.* Observation of a new particle in the search for the Standard Model Higgs boson with the ATLAS detector at the LHC. *Phys. Lett. B* **716,** 1–29. arXiv: 1207.7214 [hep-ex] (2012).
7. Bilenky, S. M. *Bruno Pontecorvo: Mister Neutrino* in *3rd International Workshop on NO-VE: Neutrino Oscillations in Venice: 50 Years after the Neutrino Experimental Discovery* (Mar. 2006), 599–609. arXiv: physics/0603039.
8. Kajita, T. ATMOSPHERIC NEUTRINOS AND DISCOVERY OF NEUTRINO OSCILLATIONS. *Proc. Japan Acad. B* **86,** 303–321 (2010).
9. McDonald, A. B. Evidence for neutrino oscillations. I. Solar and reactor neutrinos. *Nucl. Phys. A* **751** (eds Jonson, B., Meister, M., Nyman, G. & Zhukov, M.) 53–66. arXiv: nucl-ex/0412005 (2005).
10. Gronau, M., Leung, C. N. & Rosner, J. L. Extending Limits on Neutral Heavy Leptons. *Phys. Rev. D* **29,** 2539 (1984).
11. Nardi, E., Roulet, E. & Tommasini, D. Limits on neutrino mixing with new heavy particles. *Phys. Lett. B* **327,** 319–326. arXiv: hep-ph/9402224 (1994).
12. Atre, A., Han, T., Pascoli, S. & Zhang, B. The Search for Heavy Majorana Neutrinos. *JHEP* **05,** 030. arXiv: 0901.3589 [hep-ph] (2009).

13. Fernandez-Martinez, E., Hernandez-Garcia, J. & Lopez-Pavon, J. Global constraints on heavy neutrino mixing. *JHEP* **08,** 033. arXiv: 1605.08774 [hep-ph] (2016).

14. Batra, A., Bharadwaj, P., Mandal, S., Srivastava, R. & Valle, J. W. F. Phenomenology of the simplest linear seesaw mechanism. *JHEP* **07,** 221. arXiv: 2305.00994 [hep-ph] (2023).

15. Escrihuela, F. J., Forero, D. V., Miranda, O. G., Tortola, M. & Valle, J. W. F. On the description of nonunitary neutrino mixing. *Phys. Rev. D* **92.** [Erratum: Phys.Rev.D 93, 119905 (2016)], 053009. arXiv: 1503.08879 [hep-ph] (2015).

16. Escrihuela, F. J., Forero, D. V., Miranda, O. G., Tórtola, M. & Valle, J. W. F. Probing CP violation with non-unitary mixing in long-baseline neutrino oscillation experiments: DUNE as a case study. *New J. Phys.* **19,** 093005. arXiv: 1612.07377 [hep-ph] (2017).

17. Miranda, O. G., Papoulias, D. K., Sanders, O., Tórtola, M. & Valle, J. W. F. Future CEvNS experiments as probes of lepton unitarity and light-sterile neutrinos. *Phys. Rev. D* **102,** 113014. arXiv: 2008.02759 [hep-ph] (2020).

18. Centelles Chuliá, S., Miranda, O. & Valle, J. W. F. Leptonic neutral-current probes in a short-distance DUNE-like setup. arXiv: 2402.00114 [hep-ph] (Jan. 2024).

19. Tanabashi, M. *et al.* Review of Particle Physics. *Phys. Rev. D* **98,** 030001 (2018).

20. Peskin, M. E. & Schroeder, D. V. *An Introduction to quantum field theory* ISBN: 978-0-201-50397-5 (Addison-Wesley, Reading, USA, 1995).

21. Giunti, C. & Kim, C. W. *Fundamentals of Neutrino Physics and Astrophysics* ISBN: 978-0-19-850871-7 (2007).

22. Rodejohann, W. & Valle, J. W. F. Symmetrical Parametrizations of the Lepton Mixing Matrix. *Phys. Rev. D* **84,** 073011. arXiv: 1108.3484 [hep-ph] (2011).

23. Celestino-Ramírez, J. M., Escrihuela, F. J., Flores, L. J. & Miranda, O. G. Testing the nonunitarity of the leptonic mixing matrix at FASERv and FASERv2. *Phys. Rev. D* **109,** L011705. arXiv: 2309.00116 [hep-ph] (2024).

24. Schechter, J. & Valle, J. W. F. Neutrino Masses in SU(2) x U(1) Theories. *Phys. Rev. D* **22,** 2227 (1980).

25. Forero, D. V., Giunti, C., Ternes, C. A. & Tortola, M. Nonunitary neutrino mixing in short and long-baseline experiments. *Phys. Rev. D* **104,** 075030. arXiv: 2103.01998 [hep-ph] (2021).

26. Antusch, S. & Fischer, O. Non-unitarity of the leptonic mixing matrix: Present bounds and future sensitivities. *JHEP* **10,** 094. arXiv: 1407.6607 [hep-ph] (2014).

27. Langacker, P. & London, D. Mixing Between Ordinary and Exotic Fermions. *Phys. Rev. D* **38,** 886 (1988).

28. Dutta, D. & Roy, S. Non-Unitarity at DUNE and T2HK with Charged and Neutral Current Measurements. *J. Phys. G* **48,** 045004. arXiv: 1901.11298 [hep-ph] (2021).

29. Ismail, A., Mammen Abraham, R. & Kling, F. Neutral current neutrino interactions at FASERν. *Phys. Rev. D* **103,** 056014. arXiv: 2012.10500 [hep-ph] (2021).

30. Minkowski, P. $\mu \to e\gamma$ at a Rate of One Out of 10^9 Muon Decays? *Phys. Lett. B* **67,** 421–428 (1977).

31. Yanagida, T. Horizontal gauge symmetry and masses of neutrinos. *Conf. Proc. C* **7902131** (eds Sawada, O. & Sugamoto, A.) 95–99 (1979).

32. Gell-Mann, M., Ramond, P. & Slansky, R. Complex Spinors and Unified Theories. *Conf. Proc. C* **790927,** 315–321. arXiv: 1306.4669 [hep-th] (1979).

33. Mohapatra, R. N. & Senjanovic, G. Neutrino Mass and Spontaneous Parity Nonconservation. *Phys. Rev. Lett.* **44,** 912 (1980).

34. Foot, R., Lew, H., He, X. G. & Joshi, G. C. Seesaw Neutrino Masses Induced by a Triplet of Leptons. *Z. Phys. C* **44,** 441 (1989).

35. Garnica, J. C., Hernández-Tomé, G. & Peinado, E. Charged lepton-flavor violating processes and suppression of nonunitary mixing effects in low-scale seesaw models. *Phys. Rev. D* **108,** 035033. arXiv: 2302.07379 [hep-ph] (2023).

36. Centelles Chuliá, S., Herrero-Brocal, A. & Vicente, A. The Type-I Seesaw family. arXiv: 2404.15415 [hep-ph] (Apr. 2024).

37. Forero, D. V., Morisi, S., Tortola, M. & Valle, J. W. F. Lepton flavor violation and non-unitary lepton mixing in low-scale type-I seesaw. *JHEP* **09,** 142. arXiv: 1107.6009 [hep-ph] (2011).

38. Mohapatra, R. N. & Valle, J. W. F. Neutrino Mass and Baryon Number Nonconservation in Superstring Models. *Phys. Rev. D* **34,** 1642 (1986).

39. Malinsky, M., Romao, J. C. & Valle, J. W. F. Novel supersymmetric SO(10) seesaw mechanism. *Phys. Rev. Lett.* **95,** 161801. arXiv: hep-ph/0506296 (2005).

40. Xing, Z.-z. Correlation between the Charged Current Interactions of Light and Heavy Majorana Neutrinos. *Phys. Lett. B* **660,** 515–521. arXiv: 0709.2220 [hep-ph] (2008).

41. Xing, Z.-z. A full parametrization of the 6 X 6 flavor mixing matrix in the presence of three light or heavy sterile neutrinos. *Phys. Rev. D* **85,** 013008. arXiv: 1110.0083 [hep-ph] (2012).

42. Celestino-Ramirez, J. M. & Miranda, O. G. Charged lepton-flavor violating constraints to non-unitarity in the Linear Seesaw scheme. arXiv: 2405.03907 [hep-ph] (May 2024).

43. Han, H.-c. & Xing, Z.-z. A full parametrization of the 9×9 active-sterile flavor mixing matrix in the inverse or linear seesaw scenario of massive neutrinos. *Nucl. Phys. B* **973,** 115609. arXiv: 2110.12705 [hep-ph] (2021).

44. Abreu, H. *et al.* First Direct Observation of Collider Neutrinos with FASER at the LHC. *Phys. Rev. Lett.* **131,** 031801. arXiv: 2303.14185 [hep-ex] (2023).

45. Abreu, H. *et al.* The FASER Detector. arXiv: 2207.11427 [physics.ins-det] (July 2022).

46. Ariga, A. Detecting and studying high-energy neutrinos with FASERν at the LHC. *PoS* **ICHEP2020,** 112 (2021).

47. Kling, F. & Nevay, L. J. Forward neutrino fluxes at the LHC. *Phys. Rev. D* **104,** 113008. arXiv: 2105.08270 [hep-ph] (2021).

48. Deppisch, F. & Valle, J. W. F. Enhanced lepton flavor violation in the supersymmetric inverse seesaw model. *Phys. Rev. D* **72,** 036001. arXiv: hep-ph/0406040 (2005).

49. He, B., Cheng, T. P. & Li, L.-F. A Less suppressed mu —> e gamma loop amplitude and extra dimension theories. *Phys. Lett. B* **553,** 277–283. arXiv: hep-ph/0209175 (2003).

50. Hernández-Tomé, G., Illana, J. I., Masip, M., López Castro, G. & Roig, P. Effects of heavy Majorana neutrinos on lepton flavor violating processes. *Phys. Rev. D* **101,** 075020. arXiv: 1912.13327 [hep-ph] (2020).

51. Ilakovac, A. & Pilaftsis, A. Flavor violating charged lepton decays in seesaw-type models. *Nucl. Phys. B* **437,** 491. arXiv: hep-ph/9403398 (1995).

52. Adam, J. *et al.* New constraint on the existence of the $\mu^+ \to e^+\gamma$ decay. *Phys. Rev. Lett.* **110,** 201801. arXiv: 1303.0754 [hep-ex] (2013).

53. Baldini, A. M. *et al.* The design of the MEG II experiment. *Eur. Phys. J. C* **78,** 380. arXiv: 1801.04688 [physics.ins-det] (2018).

54. Aubert, B. *et al.* Searches for Lepton Flavor Violation in the Decays tau+- —> e+- gamma and tau+- —> mu+- gamma. *Phys. Rev. Lett.* **104,** 021802. arXiv: 0908.2381 [hep-ex] (2010).

55. Altmannshofer, W. *et al.* The Belle II Physics Book. *PTEP* **2019** (eds Kou, E. & Urquijo, P.) [Erratum: PTEP 2020, 029201 (2020)], 123C01. arXiv: 1808.10567 [hep-ex] (2019).

56. Casas, J. A. & Ibarra, A. Oscillating neutrinos and $\mu \to e, \gamma$. *Nucl. Phys. B* **618,** 171–204. arXiv: hep-ph/0103065 (2001).

57. De Salas, P. F. *et al.* 2020 global reassessment of the neutrino oscillation picture. *JHEP* **02,** 071. arXiv: 2006.11237 [hep-ph] (2021).

58. Celestino-Ramírez, J. M., HernándezTomé, G., Miranda, O. G. & Peinado, E. Non-unitary limits on different textures for low-scale seesaw models. arXiv: 2408.13232 [hep-ph] (Aug. 2024).

59. Frampton, P. H., Glashow, S. L. & Marfatia, D. Zeroes of the neutrino mass matrix. *Phys. Lett. B* **536,** 79–82. arXiv: hep-ph/0201008 (2002).

60. Ludl, P. O., Morisi, S. & Peinado, E. The Reactor mixing angle and CP violation with two texture zeros in the light of T2K. *Nucl. Phys. B* **857,** 411–423. arXiv: 1109.3393 [hep-ph] (2012).

61. Alcaide, J., Salvado, J. & Santamaria, A. Fitting flavour symmetries: the case of two-zero neutrino mass textures. *JHEP* **07,** 164. arXiv: 1806.06785 [hep-ph] (2018).

62. De La Vega, L. M. G., Ferro-Hernandez, R. & Peinado, E. Simple A_4 models for dark matter stability with texture zeros. *Phys. Rev. D* **99,** 055044. arXiv: 1811.10619 [hep-ph] (2019).